

DISCLAIMER:

This document does not meet the
current format guidelines of
the Graduate School at
The University of Texas at Austin.

It has been published for
informational use only.

Copyright

by

Luke Robert Nicolini

2016

The Thesis committee for Luke Robert Nicolini

Certifies that this is the approved version of the following thesis:

**Development and Analysis of Stretchable Electronics in
Biopotential Monitoring**

Approved by

Supervising Committee:

Nanshu Lu, Supervisor

Dragan Djurdjanovic

Development and Analysis of Stretchable Electronics in Biopotential Monitoring

by

Luke Robert Nicolini, B.S.M.E.

Thesis

Presented to the Faculty of the Graduate School

of the University of Texas at Austin

in Partial Fulfillment

of the Requirements

for the Degree of

Master of Science in Engineering

The University of Texas at Austin

May 2016

Acknowledgements

I would like to thank the US Office of Naval Research, for the funding (ONR N00014-16-1-2044) that has made this Thesis and my graduate education possible. I would also like to thank my Advisor Dr Nanshu Lu, for her help and expertise from my Undergraduate through my Masters career, and for her support both professionally and emotionally which allowed me to undertake my research of interest. Thank you to my Co-Supervisor Dr Dragan Djurdjanovic, whose expertise in modeling of systems was crucial in the creation of new modeling techniques in this Thesis. I would also like to thank my many colleagues in both the Lu Group and Djurdjanovic group, for their hard work and cooperation which allowed for better and more thorough research.

On a personal note, I would like to thank my high school science teacher Mrs. Kathy Celestine, whose enthusiasm for Science inspired me to pursue my degree in Engineering. I would also like to thank my mother Paula Nicolini, who always pushes me to achieve the best I can, and does everything to help me along the way. Thank you to my father Andrew Nicolini, who works long hours and drives long commutes so that my sisters and I are able to afford a good education and lifestyle. Finally, I would like to thank my girlfriend Sara Benner, for supporting me on the days where it was difficult and the desire to continue waned, and for always believing in me and my ability to accomplish my Master's program and beyond.

Abstract

Development and Analysis of Stretchable Electronics in Biopotential Monitoring

Luke Nicolini, M.S.E.

The University of Texas at Austin, 2016

Supervisors: Nanshu Lu

In this Thesis, stretchable electronics are studied and developed, with a focus on the epidermal monitoring of biopotentials for healthcare and other applications. Conventional manufacturing processes for stretchable electronics are time and cost intensive. A novel manufacturing method to create stretchable electronics is developed, in which a cutter plotter is used to directly shape thin metal films, in order to produce stretchable designs. The limits of the manufacturing process are investigated and recorded, both in terms of the cutter plotter capabilities and in the use of different materials and substrates for the thin-film device. The thin, stretchable devices are also tested in a wide variety of data collection situations, including measuring of a variety of biopotentials including ECG, EMG, and EEG. The new Epidermal Sensor Systems created with the Cut-and-Paste manufacturing method perform equal to or better than conventional electrodes. Thus the cut-and-paste method is determined to be a novel and more cost effective method to produce stretchable sensors.

Stretchable sensors we produce can match the thickness and mechanical stiffness of human epidermis, and can hence be laminated and fully conformed on human skin like a temporary transfer tattoo for long-term biopotential monitoring including electrocardiogram (ECG), electromyogram (EMG), and electroencephalogram (EEG). Such epidermal sensors have enabled the investigation of muscle fatigue and recovery over time. An Autoregressive Moving Average (ARMAX) model is developed in order to map between forearm flexor muscle EMG and the grip force of the corresponding hand. The fit of this model is tracked over the course of fatigue, and changes in the model are analyzed to provide useful trends with which to measure and follow muscle fatigue patterns. The epidermal sensor is found to be equivalent to conventional electrodes for muscle fatigue monitoring, while being more comfortable and durable. Further, the ARMAX modeling procedure is proven to have useful results in terms of modeling of forearm muscle fatigue.

Overall, this research contributes to the field of stretchable electronics and their applications for biopotential monitoring.

Table of Contents

List of Tables	iv
List of Figures	iv
Section 1: Introduction	1
Section 2: Wearable Electronics	3
Section 2.1: Bendable Electronics.....	3
Section 2.2: Stretchable Electronics.....	6
Section 2.3: Biological Considerations & Constraints	9
Section 3: “Cut-and-Paste” Manufacture of Multiparametric Epidermal Sensor Systems (ESS)	17
Section 3.1: Cut-and-Paste Method	17
Section 3.2: Sensor Design & Mechanical Properties	22
Section 3.3: Physiological Measurement Capabilities	29
Section 4: Quantification of Forearm-Hand Muscle Dynamics Over Time Using Stretchable Sensors ...	32
Section 4.1: Sensor Design	33
Section 4.2: Experimental Setup and Procedures	35
Section 4.3: Results and Discussion	39
Section 5: Conclusion	46
References	48

List of Tables

Table 1: Thickness and Young's Moduli of Materials and Designs	24
--	----

List of Figures

Figure 1: Example of Bendable Electronics in Bending	4
Figure 2: Schematic of Bending.....	5
Figure 3: Schematic of Linear Serpentine	8
Figure 4: Skin Layer Composition, Dermis and Epidermis	10
Figure 5: Equivalent Electric Circuit of Human Skin	11
Figure 6: Effect of Exfoliation of Skin Surface on Skin Impedance	11
Figure 7: Manufacturing Schematic for Cut-and-Paste Thin-Film Manufacturing	18
Figure 8: Resolution Test of Cut-and-Paste Method	20
Figure 9: Ribbon-width Testing.....	21
Figure 10: Effects of Blade Integrity on Cut Serpentine	22
Figure 11: All-In-One Epidermal Stretchable Sensor Device.....	23
Figure 12: Stretchability Tests of Sensor Designs.....	26
Figure 13: ESS on Different Substrates	27
Figure 14: Deformation vs Reliability Testing	28
Figure 15: Example EP Measurements	30
Figure 16: Sun-Type Electrode Design, Device and Deformation on Skin	34
Figure 17: Sun-type Electrode on Arm with Hand Grip Device, with Example Measurements	36
Figure 18: Fatigue and Recovery of Forearm Muscle with Sun-Type Electrodes	39
Figure 19: Fatigue and Recovery of Forearm Muscle with Conventional Electrodes	40
Figure 20: Fatigue and Partial Recovery of Forearm Flexor Muscle	41
Figure 21: Repeated Fatigue and Recovery of Forearm Flexor Muscles	42
Figure 22: Correlation Residuals for Sun-type and Conventional Electrode Measurements	44

Section 1: Introduction

As technology continues to advance and electronic devices become smaller, there is more and more of a focus on portability and ease of use when it comes to new devices.

As an example, phones have transitioned from wall-mounted devices to wireless mounts to pocket phones, and now are so small and powerful they rival modern computers while still fitting inside of a pocket. New technologies, especially electronics, should be portable and easy-to-use, to make the experience greatest for the end user.

Personal health has also experienced a surge in interest, and new portable technologies are making tracking one's own health easier than ever. The popular FitBit is one example: a wristband device that tracks the user's steps and sleep patterns, while also allowing for customization of goals and connecting with other users to create both a helpful tool and a support group to encourage personal health. While the FitBit and other similar devices have already proven popular, they are limited in the type and accuracy of data they may collect, due to the fact that they cannot interface directly with the skin surface in a reliable matter.

What this thesis will explore is the creation and application of an Epidermal Sensor Systems (ESS's). Pioneered by the John Rogers group at the University of Illinois, epidermal stretchable electronics are ultra-thin devices which rest directly on the human skin. The devices take advantage of special shapes that allow normally rigid metals to be stretched further than human skin is capable. The principles behind these properties will be explained in greater detail in Section 2. Furthermore, thanks to their intimate contact with the human body, they can be used to measure a wide variety of different health signals, such as Electrocardiograms (ECG), electromyograms (EMG), skin

hydration levels, breathing rates, and much more. The simple properties behind the stretchability of the device also allowed us to invent a new manufacturing method much faster than traditional nanomanufacturing. The design, manufacturing, and capabilities of our new ESS device will be further explored in Section 3. Finally, a large advantage the ESS has over traditional sensors, such as conventional electrodes, is durability gained by the device's conformability and non-invasive nature. The flexibility allows for natural movement of the subject, allowing for more natural physiological signals to be captured and analyzed. To confirm this hypothesis, we performed several tests to build an accurate model between the EMG of the forearm and the associated Hand Grip Force (HGF) and analyze the recovery of a muscle for after exhaustive workout. The details and procedures of these experiments, as well as results comparing ESS and conventional electrode measurements, are found in Section 4.

The following section will delve deeper into the research preceding current wearable electronic technologies, as well as the current state-of-the-art. The section will also tie all this together and explain the influence on our new technology, and where further work may take it.

Section 2: Wearable Electronics

In this section, the history and concepts behind wearable electronics, both bendable and stretchable, are covered. Section 2.1 will review bendable electronics, devices which are able to curve and bend with motion without losing integrity or functionality. Section 2.2 will cover the newer field of stretchable electronics, devices which are capable of withstanding large strains without loss of functionality. Finally, Section 2.3 will cover Biological Considerations & Constraints needed when applying these two types of technology to a living animal or person.

Section 2.1 Bendable Electronics

Bendable Electronics are devices manufactured in such a manner that they can withstand high curvature without losing function or form. The earliest known bendable electronic schematics were by Albert Hanson in an English patent in 1903, which described printing flat metal conductors onto paraffin coated paper; these patents were rediscovered by Dr. Ken Gilleo [1]. Since then, innumerable different patents and ideas of bendable electronics have been invented and published, with nearly all of them having a similar philosophy: placement of thin, rigid material on a flexible substrate.

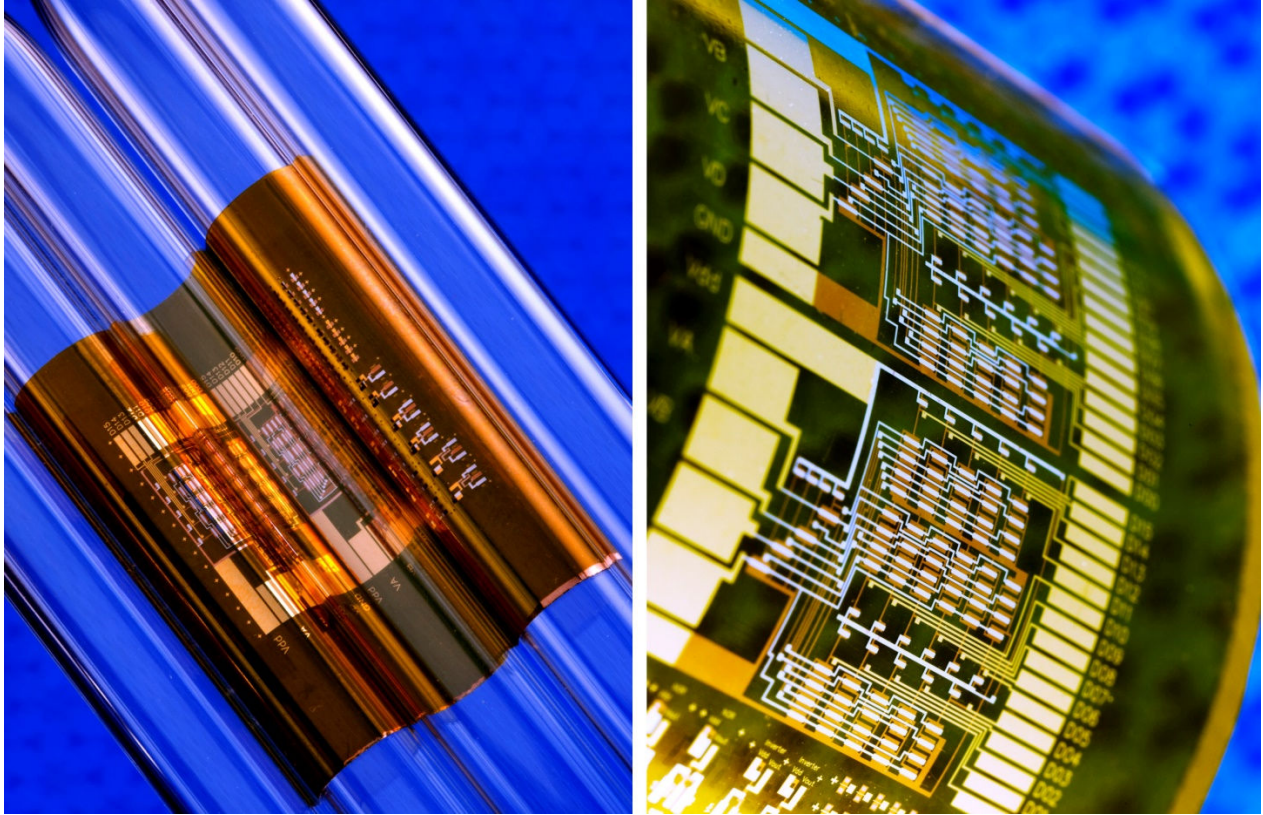


Figure 1: Example of Bendable Electronics in Bending

Metals, the most common and arguably most effective conductors for electronics, are capable of small-scale bending naturally [2,3]. However, the most commonly used metals cannot survive under conditions of extreme bending, and as such new materials or methods are required [2,4-8].

The mechanics of bending involve differing kinds of stress applied to the materials, both tension and compression. As viewed in Figure 2, materials on one side of a bend are

subjected to compressive forces, while the other side is subject to tension [2].

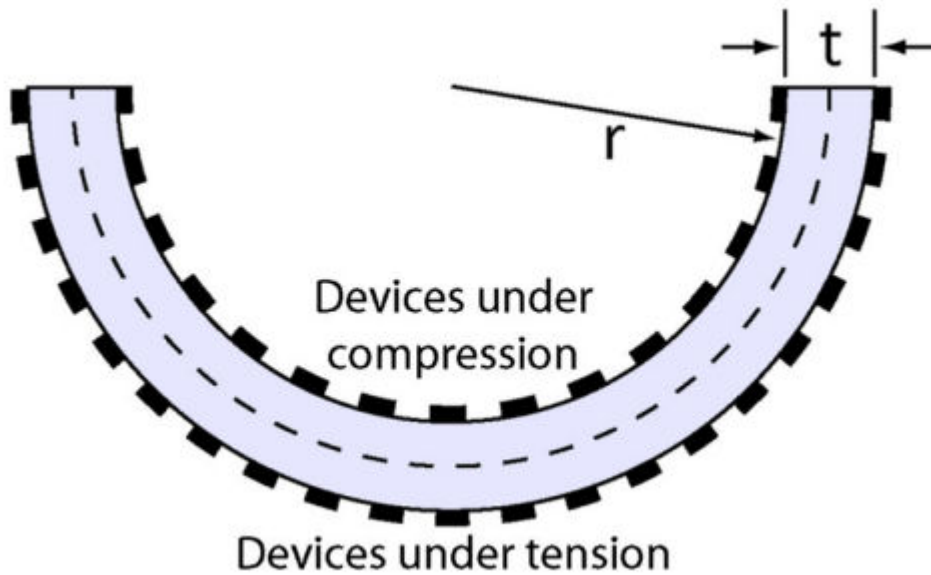


Figure 2: Schematic of Bending [2]

For a thin film of circuit material placed on a substrate, the strain experienced due to compressive or tensile forces is affected by both the thicknesses of the materials and the relative Young's Moduli. For a homogenous bar under bending, the strain at the top or bottom of the bar can be calculated with Equation 1.

$$\epsilon_{Top/Bottom} = \frac{t}{2r} \quad (1)$$

In Equation 1, t is the thickness of the bar and r is the radius of curvature. Note that the strain here is independent of any material properties of the bar, and is instead purely based on geometry. For a non-homogenous system, such as a thin film of electrical

material on a flexible substrate, the strain on the tensile surface of the film can be found using Equation 2.

$$\epsilon_{Top} = \left(\frac{d_f + d_s}{2r} \right) \frac{1 + 2\eta + \chi\eta^2}{(1 + \eta)(1 + \chi\eta)} \quad (2)$$

In Equation 2, d_f is the thickness of the thin-film material, d_s is the thickness of the substrate, $\eta = d_f/d_s$, and $\chi = Y_f/Y_s$, the ratio of Young's Moduli. Based on these equations, a smaller Young's modulus for the substrate, or a smaller thickness of the film, will lead to smaller strain and higher possible curvature [9].

In order to reduce strain applied to the circuit even further, many bendable electronic circuits aim to place the rigid electrical components at the neutral line between the two surfaces, where the materials experience neither tension nor compression. A thin film of circuitry material will lie of the neutral plane if, for substrate S and encapsulation layer E, with Young's Moduli and thicknesses Y_E , Y_S , d_E , and d_S , Equation 3 is true [9].

$$Y_E d_E^2 = Y_S d_S^2 \quad (3)$$

Sandwiched in this way, normally rigid electronic components can bend to incredibly small radii, even to the point of folding over; the only constraint is the strain tolerance of the substrate and encapsulating materials, rather than the circuit itself [9]. These technologies allow for the creation and application of normally unbendable materials like metals or silicon wafers to be adapted into flexible devices for use in research, healthcare science, or elsewhere.

Section 2.2: Stretchable Electronics

Stretchable electronic devices are those in which the structure is able to withstand large amounts of strain while maintaining functionality, including cyclic strains. As discussed in section 2.1, the devices incorporated into bendable electronics do experience strains due to bending mechanics, but stretchable electronics are distinct in that the amount of strain induced is of a higher magnitude, from 30% to as high as several hundred percent. In comparison to bendable electronics, stretchable electronics is a relatively newer field. There are two main methods to create stretchable electronic devices: One is top-down, in which normally rigid materials are patterned in such a way as to increase stretchability, and the other is bottom-up, in which new materials are developed to have favorable electrical properties while having larger strain tolerance [10]. The Rogers group of the University of Illinois has pioneered stretchable electronics for the last decade. One major breakthrough used in much of their, research as well as the devices featured in Sections 3 and 4, is the development of a thin, serpentine pattern, whose shape allows for large strains along the device axis thanks to buckling action of the device [11]. Figure 3 shows an example of a linear serpentine structure, as well as its relevant geometric variables, being Arc Radius (R), Arc Length (l), Arc Angle (a), and Ribbon Width (w) [12].

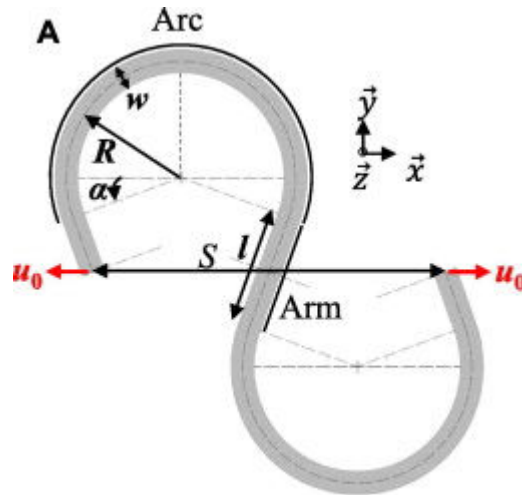


Figure 3: Schematic of Linear Serpentine

Several methods are used to allow the materials to stretch to large strains. Patterning of normally rigid materials, such as metals or silicon, into meandering shapes rather than straight lines allow the material to deform and twist during stretch, rather than yield [2, 13]. Another method involves prestrain of the substrate, such that the material is naturally buckled out of plane during rest, and “straightens out” during strain [10]. However, using this method limits the device to stretching which is less than the substrate prestrain, or else further stretching will be applied to the rigid material’s Young’s modulus [2]. A third method is to create special nanomaterials with properties of both stretchability and desired electrical properties. One example is the dispersion of conductive particles in a flexible matrix, to take advantage of the conductive nature of the particles while allowing for strain tolerance of the matrix [10]. The stretchability of a given design is difficult to calculate, and is normally found either through complex computer modeling or real-world stretchability testing. Details on some testing methods used will be given in Section 3, when discussing the design and parameters of the patterned serpentine patch used in the experiments.

Section 2.3 Biological Considerations & Constraints

One of the main advantages of ultrathin stretchable electronics, the advantage highlighted in this document, is the ability to be placed directly onto the surface of the human skin (known as epidermal electronics). Because the device interfaces with and gathers data directly from the human body, important parameters and functions of the human skin must be considered. The first is most obviously the stretchability of human skin during normal motion; as long as the device can stretch farther than the skin it is placed on, there is no concern about device malfunction, as the skin would fail before the device. Skin can withstand strains of up to 30% before failure [14]. Many stretchable electronics are capable of far greater strains, including the devices featured in this document, as will be demonstrated in Section 3.

When collecting certain data, such as biopotentials, the electrical properties of the skin are important to proper device design and placement. The human skin is made of multiple layers, which can be grouped into two main categories: the outer epidermis, and the inner endodermis. The layers of the skin are displayed in Figure 4.

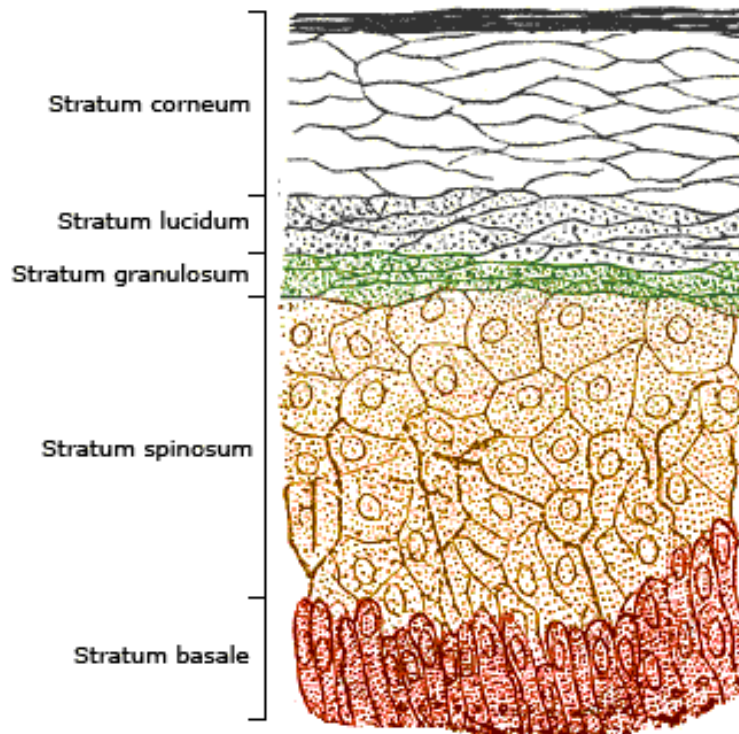


Figure 4: Skin Layer Composition, Dermis and Epidermis

The epidermis, or Stratum corneum, is made up of dead, dry skin cells, and serves as the body's shielding outer layer [15]. This layer has much larger impedance when compared with the endodermis, which is composed of live cells and as a result has higher levels of conductance. Figures 5 and 6, reproduced from a study by Yamamoto *et al* in 1976, show an equivalent circuit diagram of the human skin, and the effect of peeling away of the stratum corneum on impedance measurements (in Figure 6, the number in parentheses is the number of times the skin has been peeled using ordinary cellulose tape) [16].

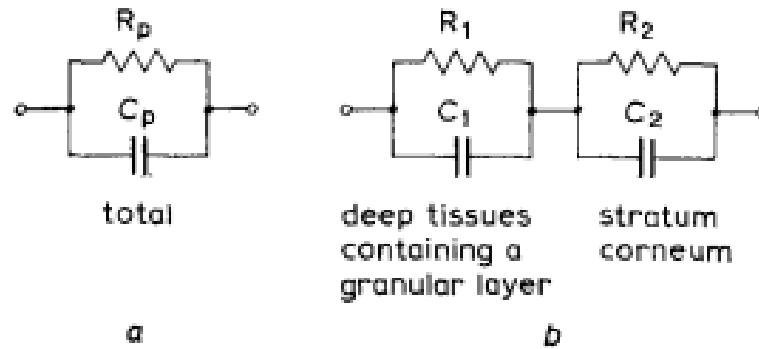


Figure 5: Equivalent Electrical Circuit of Human Skin [16]

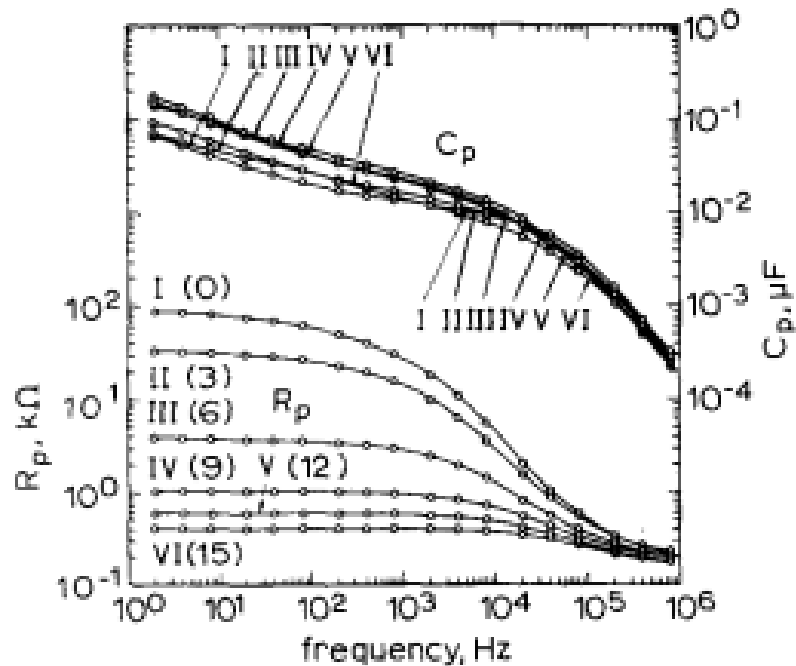


Figure 6: Effect of Exfoliation of Skin Surface on Skin Impedance [16]

Inspired by the properties shown in Figure 6, one method to reduce impedance during measurement is to pretreat the skin, by abrading it with a rough material to remove the stratum corneum. It is found that a simple alcohol wipe abrasion of the skin is sufficient when measuring Electromyography (EMG) signals on the surface of the skin while simple dry-electrodes on skin with no preparation were insufficient [17].

When placing the device to gather biopotentials, placement of the device must be considered, especially when comparing two sets of data from experiments on different subjects or using different electrodes. For electromyography (EMG) signals, the electrodes should be placed on the muscle of interest; however, it has been found that changing the relative positions on the muscle has no effect on the gathered EMG signals [18]. Further testing of this result is done in Section 4, where two collection setups are tested simultaneously in alternating positions to determine reliance on position. For the purposes of electrocardiogram (ECG) measurement, the device shown in Section 3 uses a similar design to that employed by the Rogers group, of placing the measurement, reference, and ground electrodes axially with one another separated by small distance, and placed directly above the heart [19]. Further details on its construction are explained in the following sections.

For long-term measurements on the skin, biocompatibility must also be ensured such that the device does not have any harmful effects on the end user. Gold has a proven record of being safe for use with the human body [20], as well as desirable electric properties; it has been selected as the conductor for our electrodes. Further testing on the properties of gold for the purposes of biopotential acquisition is expanded in Section 3.

In the study of muscle fatigue, many different methods have been developed to quantify the degradation of the muscle with exertion. One of the most basic methods is known as the “mechanical manifestation of muscle fatigue”, which is defined as “failure to maintain the required or expected force” [21]. This approach solely looks at outputs of muscle activity, such as force generated, and a drop in expected baseline activity is taken as a

sign of fatigue. While this method is very simple and easy to implement, it suffers from a lack of consistency, as output can be affected by non-physical factors such as motivation [22]. Another method, commonly used in professional sports, is to estimate fatigue by measuring the lactate concentration of blood at determined intervals during an exercise. Due to the nature of collecting and analyzing blood samples, with this method it is not possible to measure fatigue in real time. In addition, the collection of blood samples is invasive and requires experienced caretakers to ensure safety for the test subject. This method cannot target individual muscles, but rather gives an estimation of overall body fatigue.

The most popular and useful strategy to measure muscle activity and fatigue has been the use of surface Electromyography (sEMG). It has been shown that the biological and physical characteristics of fatigue are also reflected in the properties of EMG signals collected on the surface of the skin [23]. While this method is restricted to measurement only of muscles just below the skin, it has numerous advantages which make it the preferred method of monitoring muscle fatigue: non-invasiveness, applicability *in situ*, real-time capability, ability to target a specific muscle, and correlation with biological and physical factors [24].

The methods available to process gathered EMG data can be classified into two main camps: time-domain methods and frequency domain methods [24]. Time-domain methods aim to analyze the EMG signal itself. This is usually accomplished by measuring either EMG amplitude or Zero-crossing rate. EMG amplitude consists of two different parameters: the mean absolute value (MAV) and the Root-mean square value (RMS), calculated as Equations 4 and 5, respectively.

$$\text{MAV} = \frac{1}{N} \sum_{i=1}^N |x_i| \quad (4)$$

$$\text{RMS} = \sqrt{\frac{1}{N} \sum_{i=1}^N x_i^2} \quad (5)$$

In Equations 4 and 5, x_i is the sample taken at time i , and N is the total number of samples in the epoch. Tracking of these two values over time can lead to trends which indicate fatigue of the muscle. While useful, these methods are prone to variation based on types of machines used to collect the data, and as such these EMG amplitude methods are usually combined with other methods, rather than used alone, to analyze fatigue. Another commonly used method is the Zero-crossing rate (ZCR) of the signal, defined as half the number of times the signal crosses the zero axis [25]. While this method produces results close to those found in other time-domain methods, it is highly dependent on the Signal-to-Noise ratio of the collected EMG, and as such has generally been abandoned for the purposes of analyzing EMG.

Frequency domain methods are common in modern EMG analysis, particularly Fourier-based spectral estimators. In these methods, EMG is assumed to be a zero mean wide sense stationary (WSS) process. While this assumption is good for short-term muscle movement, the change in muscle dynamics corresponding to fatigue is inherently non-stationary, and as such these basic methods are limited. However, the Fourier-based methods still provide useful analysis of muscle activity, and can detect the change in

muscle dynamics associated with fatigue, limited by the inability to quantify degree of fatigue. For example, Roy et al. has demonstrated the ability of frequency analysis of EMG to detect lower back pain problems in professional rowers [26].

Parametric based spectral estimators have also shown use in measurement of muscle fatigue. Autoregressive (AR) modeling of the biceps brachii muscle during maximum voluntary contraction has shown a clear change in model parameters, which is useful for tracking of fatigue [27]. A focused study found the AR method to be a good indicator of fatigue, with the limitation of needing a high-order AR model which could be computationally heavy [28].

A combination approach of time domain and frequency domain has also been investigated. Namely, this method measures both the amplitude of the EMG signal and the shift in the frequency domain, and correlates the two with different muscle actions. Four different cases are distinguished: 1) Amplitude increases and spectrum shifts right, indicates muscle force increase, 2) Amplitude decreases and spectrum shifts left, indicates muscle force decrease, 3) Amplitude increases and spectrum shifts left, indicates muscle fatigue, and 4) Amplitude decreases and spectrum shifts right, indicates recovery from fatigue [24]. This method has shown very useful for tracking of fatigue, but provides no quantitative measure of fatigue severity.

Time-frequency modeling is another approach to EMG analysis, which attempts to lift the restriction of traditional frequency modeling which assumes the input signal to be stationary. Fatiguing of the muscle and movement of rigid electrodes relative to the muscle body during exercise causes the signal to be noticeably non-stationary, and as a

result any method assuming otherwise is only valid for very short time frames. These methods include Short-Time Fourier Transform (STFT), Wigner Distribution (WD), Time-varying Autoregressive (TVAR), and Choi-Williams Distribution [24, 29, 30, 31]. Time-frequency analysis is shown to have the most reliable methodology for measuring and quantification of muscle activity and fatigue, as well as the best robustness versus dynamic factors such as electrode movement. As a result, the Autoregressive method is expanded upon in order to include measurement of output force as well, to investigate the benefits for the modeling of muscle dynamics and fatigue. This analysis and results are located in Section 4.

Section 3: “Cut-and-Paste” Manufacture of Multiparametric Epidermal Sensor Systems (ESS)

The creation of epidermal electronics requires the precise shaping of ultrathin materials in order to create patterns that are functional, stretchable, and conformable enough to operate on the human skin. Traditional nanomanufacturing, the industry standard for the creation of ultrathin devices, is labor and equipment intensive, usually involving many different steps and the use of many different chemicals, all of which add up to a significant cost in time and money. In this section, a new manufacturing method dubbed “Cut-and-Paste” which uses entirely dry methods with countertop operation, allows for the creation of epidermal electronics in only a few minutes. The method is applicable to all types of thin metals and polymers, and creates devices which are shown to accurately measure a wide array of signals, including biopotentials, skin hydration, and surface temperature. Further applications of the technology as a strain sensor are also investigated.

Section 3.1: Cut-and-Paste Method

The Cut-and-Paste method uses a programmable cutting blade to shape a thin metal on thin polymer, followed by a series of transfers to an adhesive material to form the final device. The schematic of cut-and-paste is shown as Figure 7.

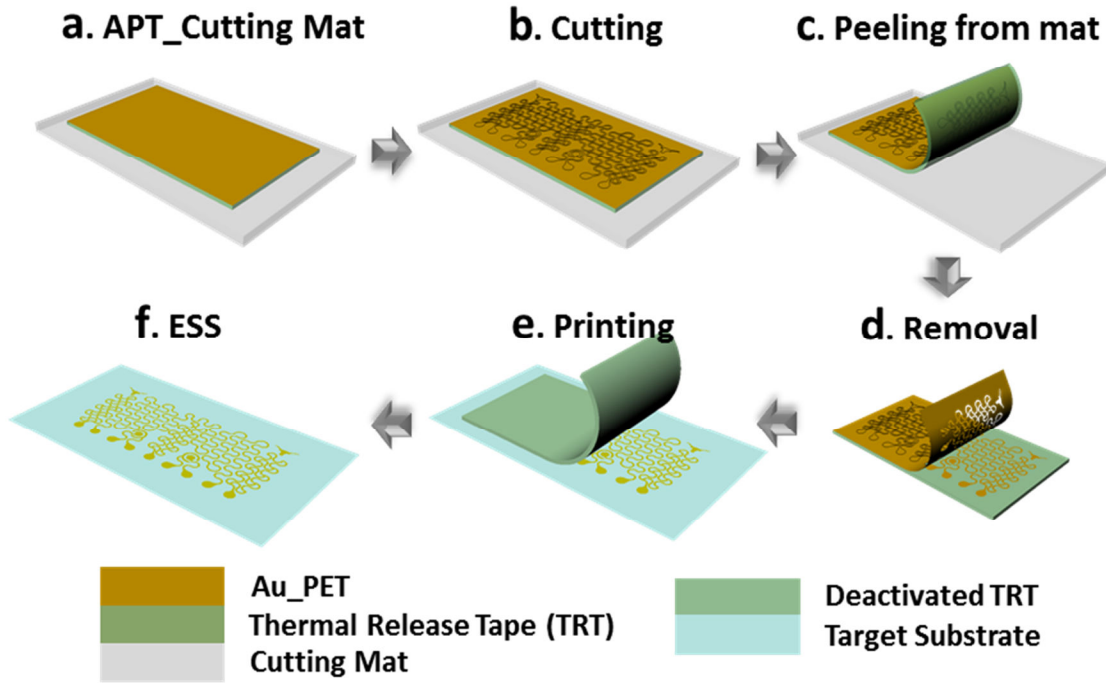


Figure 7: Manufacturing Schematic for Cut-and-Paste Thin Film Manufacturing

The process begins with a thin metal on a stiff-polymer substrate. This setup is used because it is found to always be more stretchable than simply freestanding metal sheets [32]. Two different materials were cut: gold coated polyethylene terephthalate (PET) and aluminum coated PET. The gold coated PET was created by thermal evaporation of Au with a thickness of 100 nm onto 13 μm -thick transparent PET foil. The Aluminum on PET was purchased commercially from Neptco (Pawtucket, RI), with dimensions of 9 μm -thick Al on 12 μm -thick PET laminate.

To manufacture the Au portions of the device, the Au on PET film was bonded to single-sided Thermal Release Tape (TRT) (Semiconductor Equipment Corp, USA), with Au side of the sheet contacting the TRT adhesive. The non-adhesive side of the TRT was then applied to a tacky cutting mat, to hold it in place during the cutting procedure. The cutting mat was fed into an electric cutter printer (Silhouette Cameo, USA), where

imported designs from AutoCAD allowed the printer to cut the Au on PET to desired shapes and specifications. The TRT was then peeled from the adhesive mat and placed on a hotplate set to 115 °F for 30 seconds, to allow the Au on PET film to debond slightly from the TRT. Tweezers were then used to peel off the excess gold from the design. Finally, the system was placed device-side onto an adhesive substrate, which was successfully tested to be any of the following: water-soluble temporary tattoo adhesive (Silhouette), 3M Tegaderm transparent dressing, or 3M kind removal silicon tape (KRST). The TRT was peeled away, leaving the device bonded to the adhesive substrate, with gold-side facing outwards. This creates a device which can then be applied directly to the skin to gather biopotential and other data.

The cutting machine used in this method can pattern thin films up to 12 inches by 12 inches, much larger than traditional nanomanufacturing limits available to researchers. The resulting devices can be transferred to tattoo or medical adhesives with a nearly 100% success rate, due to the support of Thermal Release Tape (TRT) during the cutting process. The entire process requires very little space and no special climate controls, while also completing in as little as 20 minutes per pass, which can yield a dozen or more samples.

Figure 8 below details the limits of resolution of the cutting machine, tested from 600 μm to 50 μm width serpentes. The material used in this testing is 9- μm -thick Al on 12- μm -thick PET foil (NEPTAPE® by NEPTCO, Inc.). At a resolution above 200 μm , the machine successfully creates the desired shape with little loss of uniformity and no compromised patterns. At 200 μm , the device created remains uncompromised, but the

uniformity of the ribbons suffers. At 100 μm and below, Figures 8e and 8f, the device itself becomes compromised, and is insufficient for use. As a result of these tests, 400 μm width ribbons were selected, to insure device integrity and uniformity.

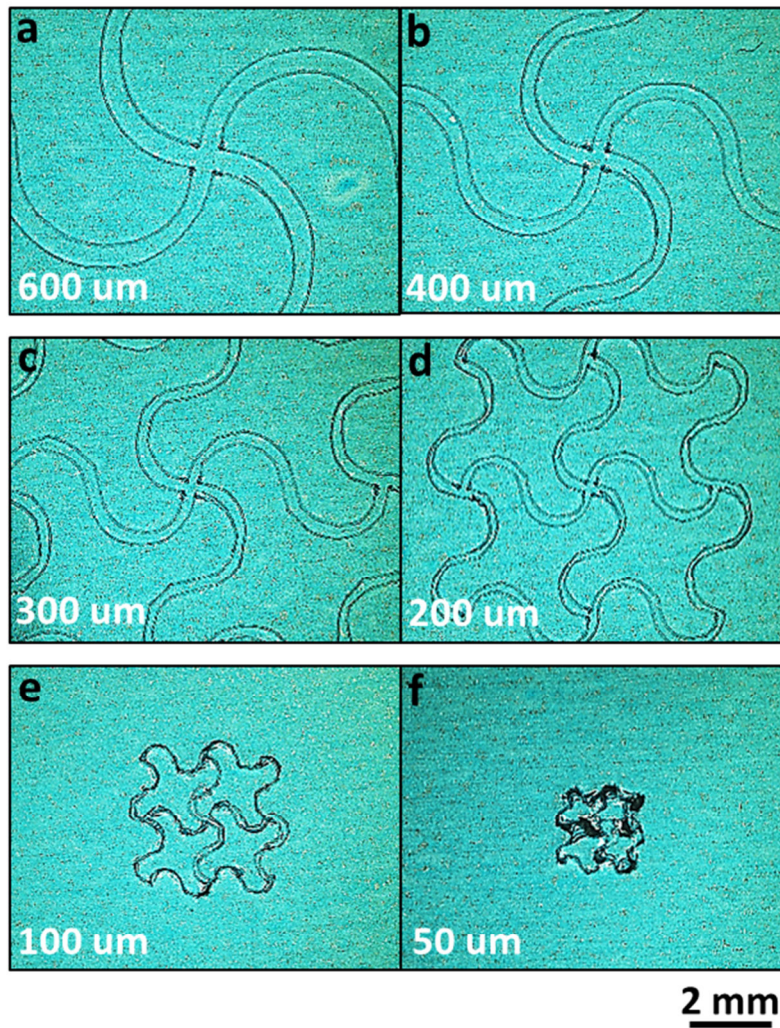


Figure 8: Resolution Test of Cut and paste method. All resolutions are measured in ribbon width.

Ribbon width uniformity tests were also performed, by measuring the median line of serpentines at evenly spaced intervals along a cut device, as shown in Figure 9. The material used in these tests is 25- μm -thick Kapton sheets (DuPont). With the cutting

machine set to produce serpentines with a width of 400 μm , the distribution of ribbon was found to be centered at 340 μm with a standard deviation of 87 μm . Thickness testing performed by profilometer found the edge of the ribbons to be less than 30 μm wide, indicating the majority of the ribbon is very flat.

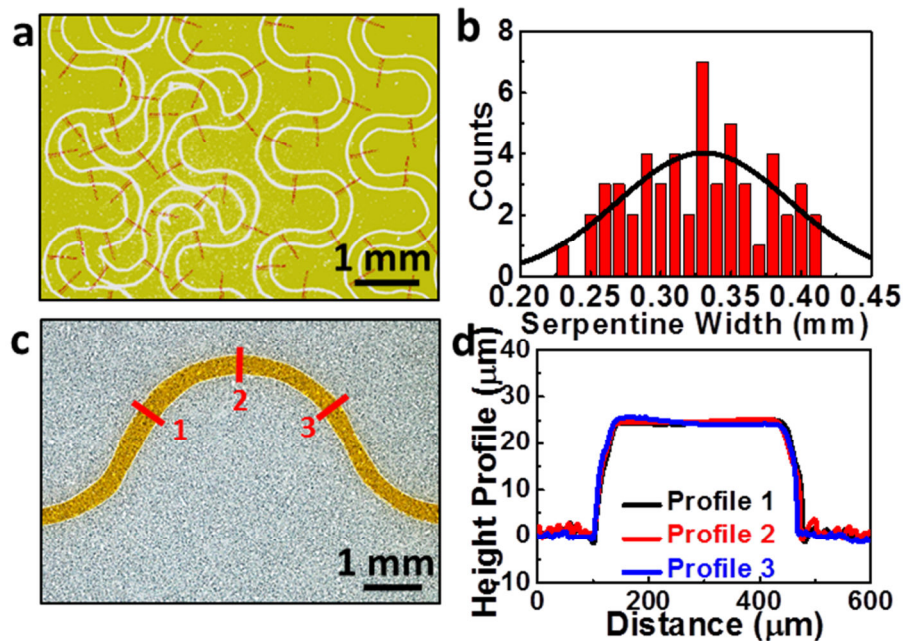


Figure 9: Ribbon width testing. a) Image of network serpentines, with measured widths. b) Plot of measured widths, with fitted normal curve. c) Location of 3 trials for ribbon thickness tests. d) Ribbon thickness across width at locations 1, 2, and 3.

Blade quality is also of critical importance to the quality of the device produced. As displayed in Figure 10, the cutting blade can become worn or destroyed, based on age of the blade, extent of use, and materials cut. In addition, the cutting thickness, speed, and sharpness parameters of the cutting machine affect the outcome of the device. As a

result of these and further studies, the ideal cutting parameters were set to sharpness=5, cutting rate=2, and thickness=1, for the best quality cuts.

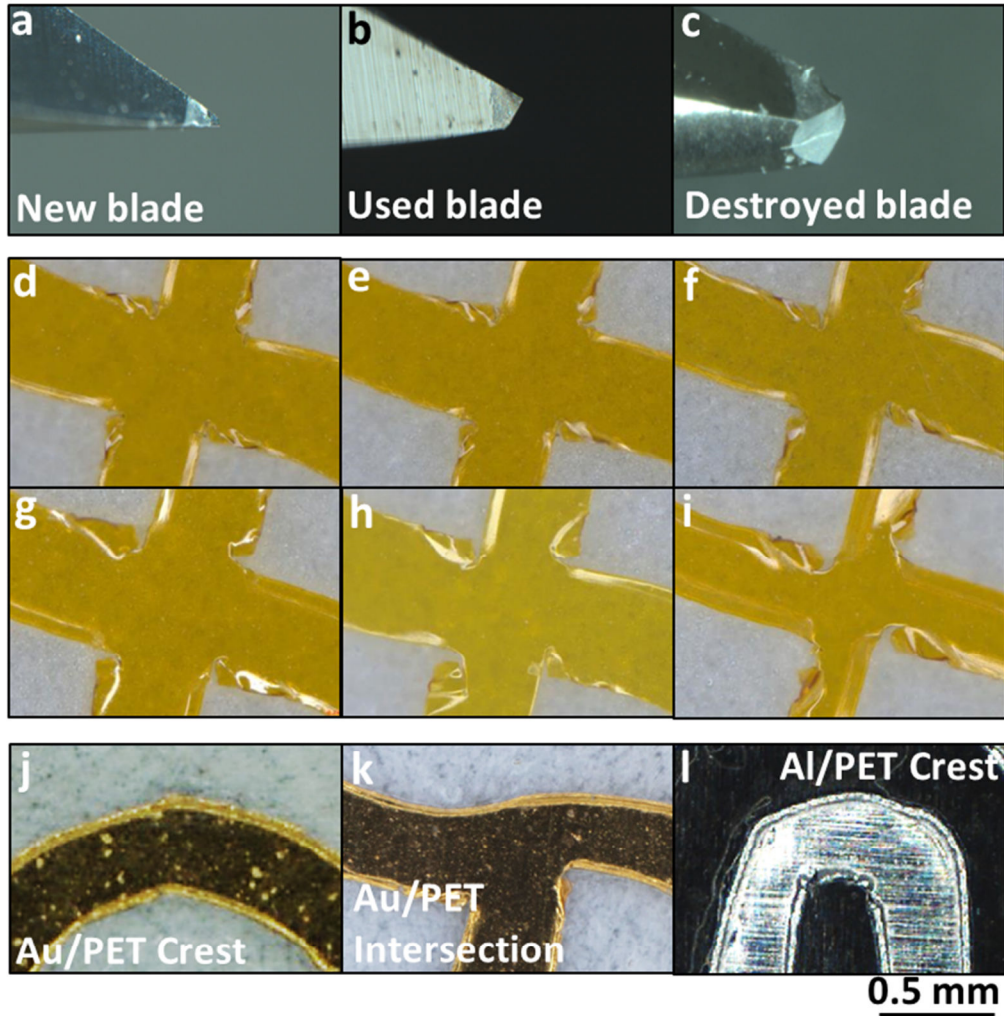


Figure 10: Effects of Blade Integrity on Cut Serpentine Networks. a), d), g) correspond to a new blade. b) e), h) correspond to a used blade. c), f), i) correspond to a "destroyed" blade. j), k), l) display cutting quality of a new blade at different portions of network

Section 3.2: Sensor Design & Mechanical Properties

The sensor created as a proof-of-concept for the cut-and-paste manufacture method is shown below in Figure 11.

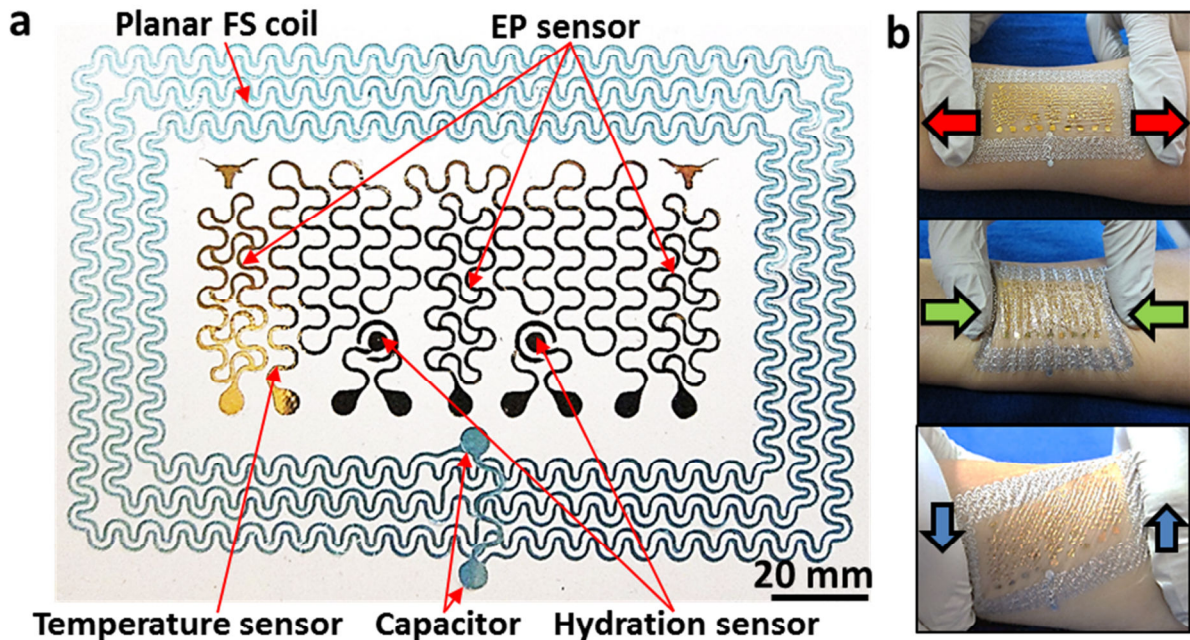


Figure 11: All-In-One Epidermal Stretchable Sensor (ESS) device. a) Layout of device with different sensors. b) Device under deformation on human skin

The device consists of three Au-based serpentine EP electrodes, one Au-based serpentine Resistive Temperature Detector (RTD), two Au-based dot-ring impedance sensors, and an Al-based planar stretchable coil. The device in figure 8 is supported on temporary tattoo adhesive material. The Au-based portions of the device are all facing inward, such that the gold may make direct contact with the skin for the purpose of collecting signal. Conversely, the Al-PET based coil is positioned with the Al facing inwards, while the PET makes contact with the skin; this is because PET has proven to be biocompatible, while Al can cause allergic reactions in some persons [33]. The three EP electrodes are spaced 2cm apart for effective recording [34]. The serpentine ribbons

are designed with a 1/5 ribbon width to arc radius ratio, to balance stretchability and surface area [35]. Due to the size constraints of the Al-coil, the 1/5 ratio was not possible, so instead a double-stranded serpentine design is used to maximize number of turns in the device, while maintaining stretchability. The RTD is patterned to have as long a path as possible while fitting within the device, in order to provide greatest total resistance and thus greatest change in resistance when exposed to differing temperatures; details of the importance of this parameter are located in Section 3.3. The overall dimension of the device area is 7.5 cm x 5cm.

The Young's moduli of all materials used in the ESS design, as well as the ESS devices themselves, were tested using a RSA-G2 dynamic mechanical analyzer (TA instruments). Each material used in either the device or the substrates were tested. The materials were cut into rectangular strips with aspect ratio 10:1 and strained in the longitudinal direction. Each material was tested five times with different specimens, and the average Young's Moduli are collected in Table 1.

Table 2: Thickness and Young's Moduli of Materials and Designs

Material	Thickness (μm)	Young's Modulus (GPa)
PET (Goodfellow)	13	4.59
Kapton (Dupont)	12.7	3.59
KRST (3M)	200	0.228
Tattoo adhesive (Silhouette)	22	0.042
ESS on Tegaderm	60	0.011
Tegaderm (3M)	47	0.007

ECR (Wacker)	120	0.003
---------------------	-----	-------

The stretchability of the materials and designs present in the device were tested using a custom tensile tester with electrical resistance measurements and webcam monitoring of strain, as viewed in Figure 12. Resistance was determined as a function of strain, and the point at which resistance explodes ($R/R_0 = 1.1$) is considered the strain-to-rupture stretchability of the material. Straight ribbons of Au on PET and Al on PET exhibit very little stretchability (13.72% and 2.89% respectively). When patterned into serpentine shaped ribbons, the stretchability of the materials greatly increased. The stretchability of the Al coil, the Au EP electrode, and the Au RTD were found to be all well above the stretchability of human skin as discussed in Section 2.3.

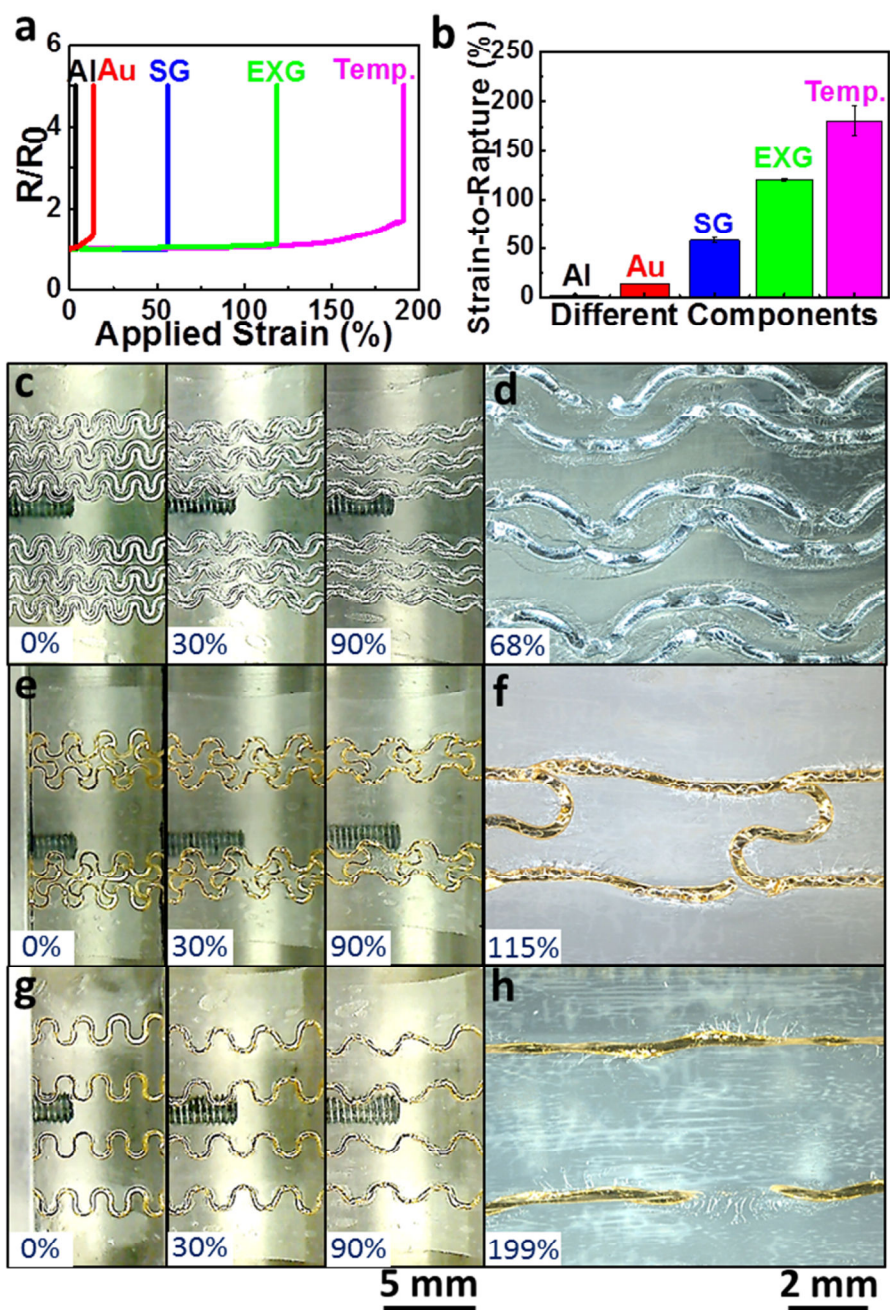


Figure 12: Stretchability Tests of Sensor Designs. a-b) Applied Strain to Rupture of Different Materials and sensor Designs. c-d) Stretchable Coil. e-f) EP sensor. g-h) Temperature Sensor

Three different substrates were tested for the purposes of supporting the ESS device, and are shown in Figure 13. Tegaderm and tattoo paper are thin, transparent, and best emulate skin-like behavior. KRST (“blue tape”) is relatively thicker, more similar to a

cloth bandage, which allows it to maintain shape even after being removed from the skin, which allows for repeated measurements even after several trials of removal and re-adhesion to the skin.

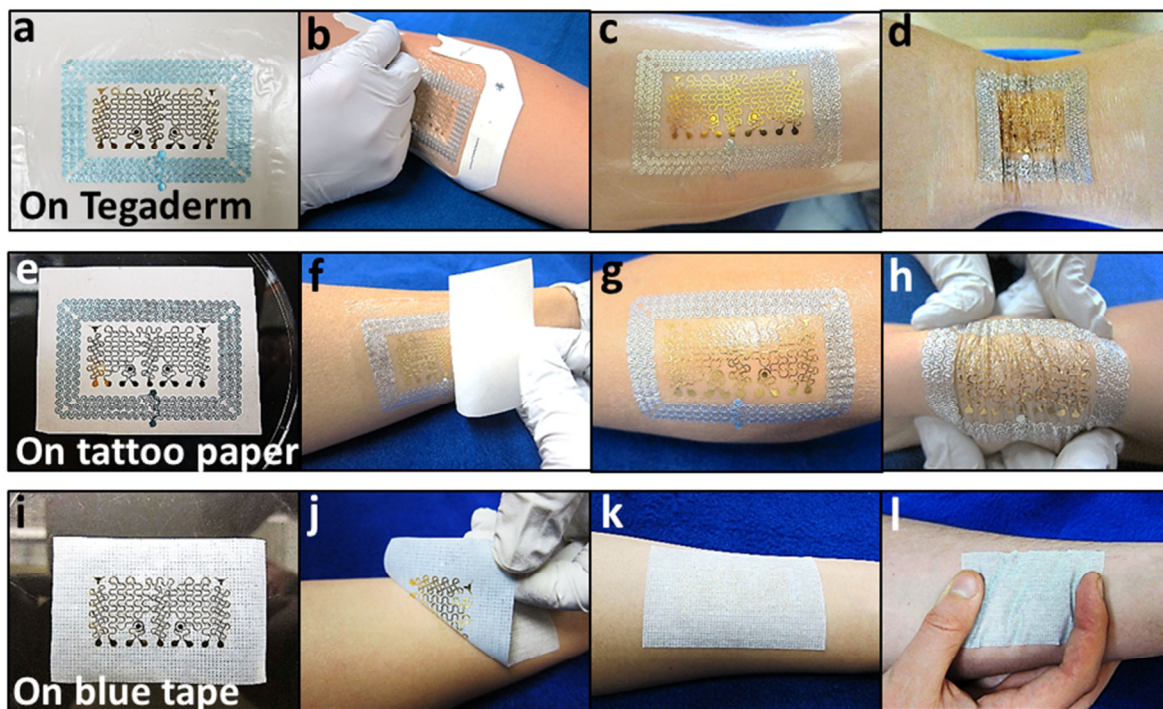


Figure 13: ESS on different substrates. a-d) Tegaderm substrate. e-h) Water-soluble tattoo paper. i-l) Medical "blue tape" bandage

In order to ensure the capabilities of the ESS device under deformation, several deformations were performed on a live subject, including stretching, compression, shearing, and poking. Resistance of the Al and Au serpentines were measured before and after the deformations, and show negligible resistance change as a result of deformation, indicating that the deformations had no effect on the electrical capabilities of the device. Examples of the tested deformations and the results are displayed in Figure 14.

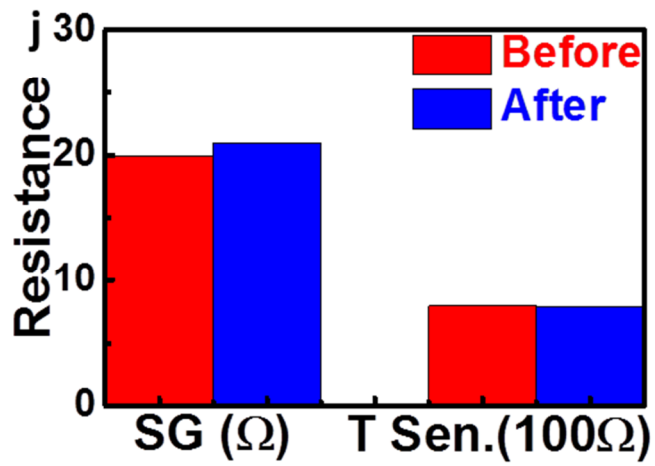
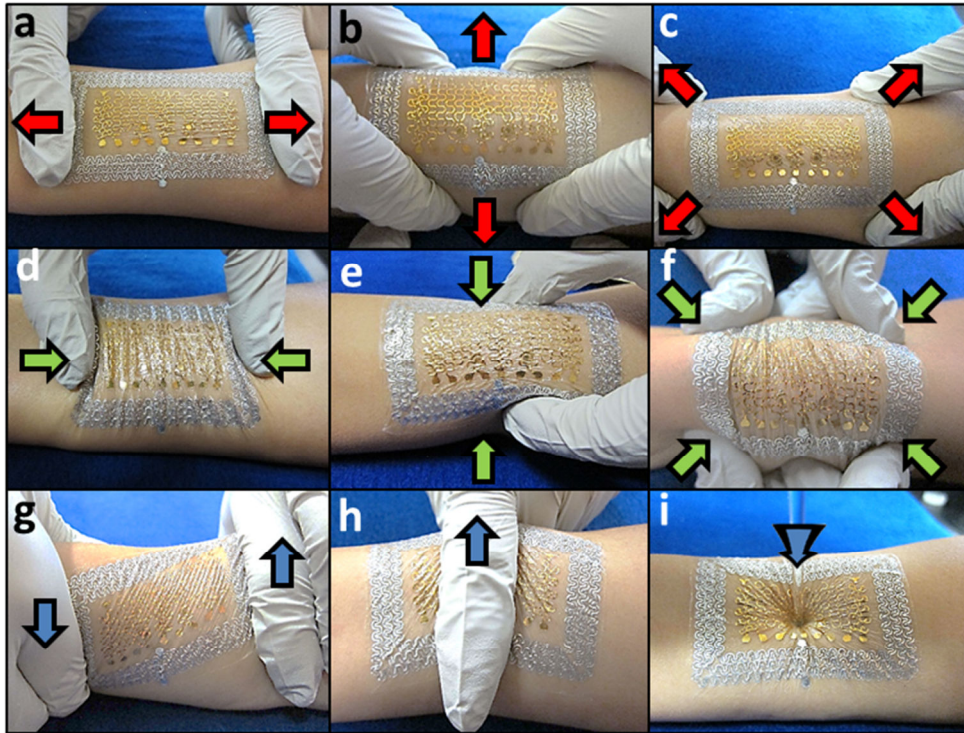


Figure 14: Deformation vs Reliability Testing. a-i) Different deformations performed on ESS while adhered to skin. j) Before and after deformation measurements of total resistance for Strain Gauge and Temperature Sensor Devices

Section 3.3 Physiological Measurement Capabilities

The multiparametric ESS design is able to successfully perform live and synchronized measurement of EP signals, skin hydration, and skin temperature. The three different types of EP measured in these trials are Electrocardiogram (ECG), Electromyogram (EMG), and Electroencephalogram (EES). Placements of the ESS to measure each type of signal, as well as example measurements, are displayed in Figure 15.

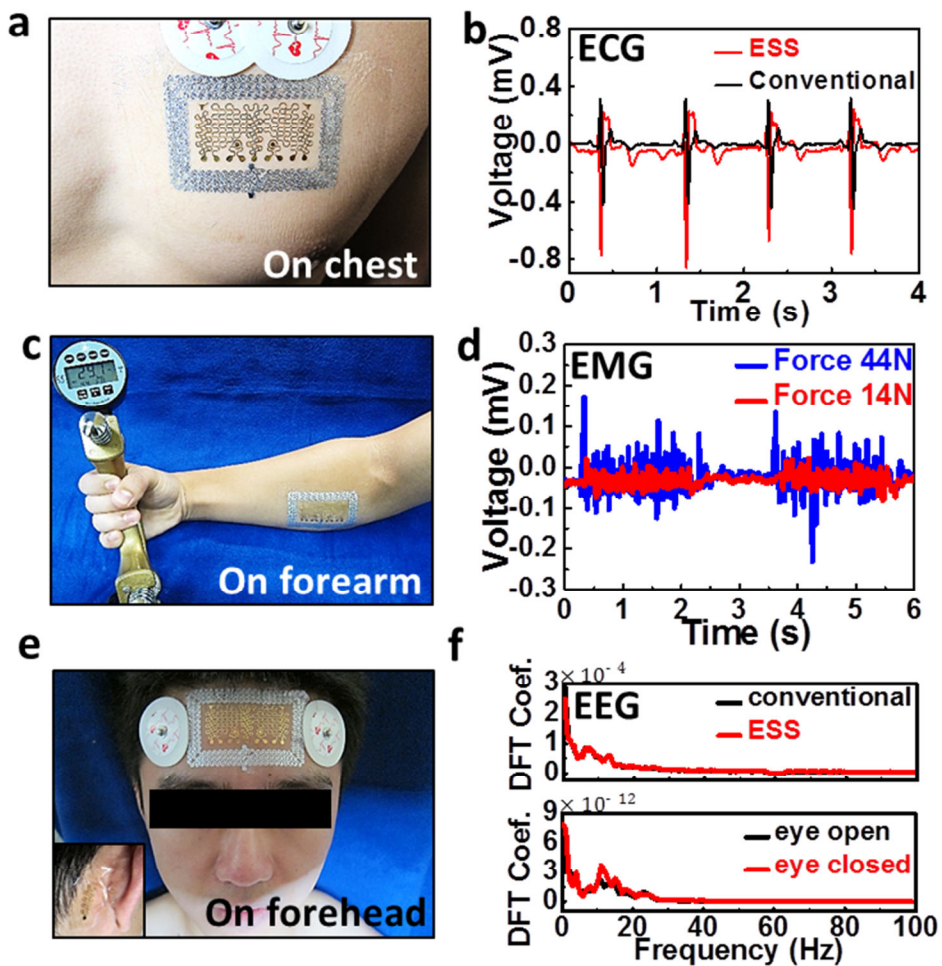


Figure 15: Example EP Measurements. a-b) EKG Measurement on the chest. c-d) EMG measurements corresponding to different grip forces. e-f) EEG taken on the forehead.

In each experiment, both the ESS EP terminals and conventional Ag/AgCl electrodes were connected to a small portable amplifier (AvatarEEG) with a common ground. For the three terminals of the ESS, the middle terminal served as the ground, while the right and left terminals served as the measurement and reference electrodes for bipolar measurement, respectively. Signals recorded were processed using a Principle

Component Analysis based algorithm [36]. The measurement of ECG shows that both ESS and conventional electrodes are able to capture the characteristic features used in modern heart care. The measurement of EMG was performed at different levels of exertion, specifically the grip force of the hand vs the flexor muscles of the forearm, and was found to be able to differentiate between these two states with a corresponding increase in amplitude of muscle EMG. Finally, EEG was measured by placing the ESS and conventional electrodes on the forehead, with references placed behind the right ear on the mastoid bone. The signals were high and low-pass filtered at 0.1Hz and 40 Hz respectively. Standard Fast Fourier transformations (FFT) were used to generate frequency spectrums of the signal. Using this method, the matchup between the EEG captured by the ESS and the conventional electrodes are virtually identical, proving the new design's ability to capture EEG while also being much softer and more conformable than traditional electrodes.

Additional tests were performed to prove the effectiveness of the Resistance Temperature Device (RTD), the dot-ring hydration sensors, and the aluminum coil. The results of these tests are displayed in brief in Figure 15. Overall, the device proved capable of measuring all parameters equal to or better than traditional methods. This proves the cut-and-paste manufacturing process to be a novel and useful method for manufacture of thin-film electronics for use in experimentation, with possible expansion to market production.

Section 4: Quantification of Forearm-Hand Muscle Dynamics and Fatigue Using Non-Restrictive Measurement Devices

The study of electromyography is a field of human biology that still harbors much potential. The first successful measurement of EMG was made in 1850 by Étienne-Jules Marey, and significant advances in the field have been made since. Yet compared to ECG or EEG, EMG has proven significantly harder to quantify, due to its irregular nature and variability from patient to patient. In this section, a new method is introduced based on Autoregressive Moving Average modeling with exogenous inputs (ARMAX) to quantify fatigue of a muscle by studying the relationship between the inputs and outputs of a muscle system, specifically the interaction between the flexor muscles of the forearm and the gripping force of the associated hand (referred to as Hand Grip Force or HGF). By measuring how the relationship changes over time, it is possible to accurately plot the change in muscle dynamics corresponding to fatigue, independent of any errors caused by human interaction.

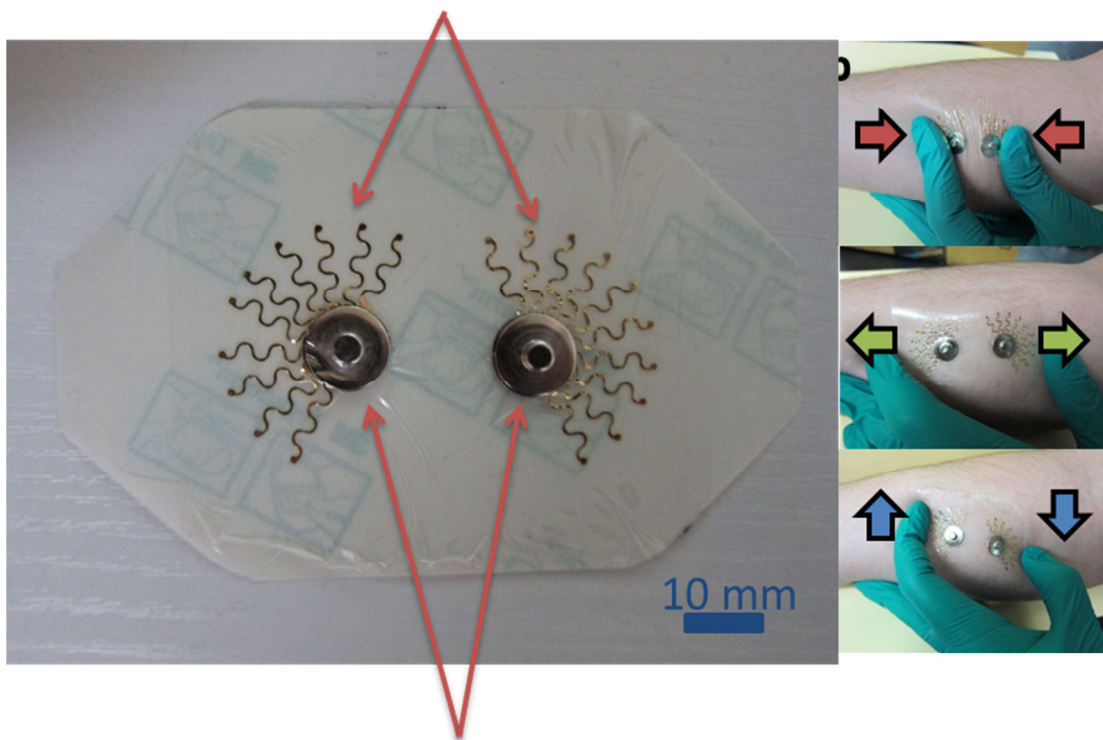
The primary motivation for using a model based analysis versus a traditional signal based analysis is that a signal based analysis assumes that the inputs and outputs are both stationary, which is not true during fatigue of the muscle. As detailed in Section 4.2, users are asked to perform maximum voluntary contraction (MVC) of the forearm muscle during data gathering, both to induce fatigue and to serve as a baseline with qualitatively obvious indication of fatigue. In an ideal scenario, the subject would be able to provide MVC for the entirety of the experiment. In reality however, subject discomfort during the experiment can cause the subject to loosen their grip, producing sub-MVC EMG and HGF results. In the case of a traditional approach, a dip in HGF or a decrease

in EMG activity could be both improperly evaluated as a sign of fatigue, when actually it is just due to the user input changing. The ARMAX model based approach to forearm performance monitoring is robust to this problem, because it quantifies the change in the relationship between the two signals, rather than the signals themselves. This allows the model to self-correct when inputs are changed, because if no degradation or fatiguing occurred the corresponding outputs will change as well but in a way that the relationship between the two remains the same. Thus, we propose that the following methods are a novel and robust method to use to measure fatigue in a muscle-force system.

Section 4.1: Sensor Design

Due to the nature of muscles to move during contraction and extension, a stretchable sensor was designed to capture EMG signals based on the Cut-and-Paste technology described in Section 3. This new design is shown in Figure 16, both stand-alone and on the target arm muscles under deformation.

Measurement Electrodes



Snap Connectors

Figure 16: Sun-type Electrode Design, device and deformation on skin.

The new design features two electrodes patterned in a radial “Sun” pattern, to increase electrode surface area while maintaining stretchability and conformability. The electrodes also each feature a snap-connector, which allows for easy connection of the electrodes to a measurement device during data capture, either by snap-on wire connectors or alligator clips. Tegaderm was chosen as the substrate for the device for its skin-like qualities, good adhesion strength, and stretchability greater than needed for muscle movement during testing. Testing done in Section 3 validates the stretchability of our device, as it uses the same filamentary serpentine designs. The following sections will demonstrate the importance of the electrode stretchability during capture of

muscle EMG. The stretchability allows both more conformal contact for truer EMG measurements, and also does not constrain the muscle during movement in order to capture the truest possible free muscle dynamics for study.

Section 4.2: Experimental Setup and Procedures

As stated previously, all experiments performed in this Section deal with the interaction between the subject's dominant hand, and the corresponding forearm flexor muscles. Data for forearm EMG was collected by our Sun patch described in Section 4.1, with a ground Ag/AgCl electrode placed elsewhere on the body. The electrodes are connected to a portable amplifier (AvatarEEG) for data collection. The HGF data is collected by a modular data collection device (Neulog) which has a bar-shaped hand dynamometer, which is squeezed to perform the measurements. A signal generator was used to produce pulse signals with frequency of 100 mHz, which were fed into both the amplifier and the modular device to serve as timing signals for synchronization of the two data sets. An example of the arm setup and a sample data set is displayed in Figure 17.

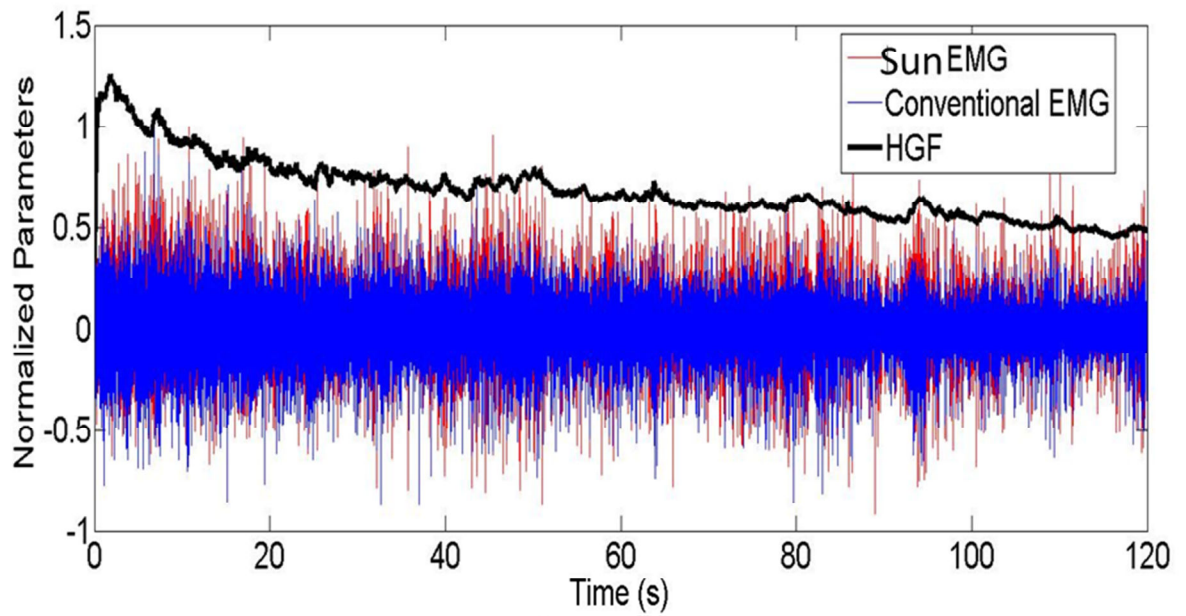
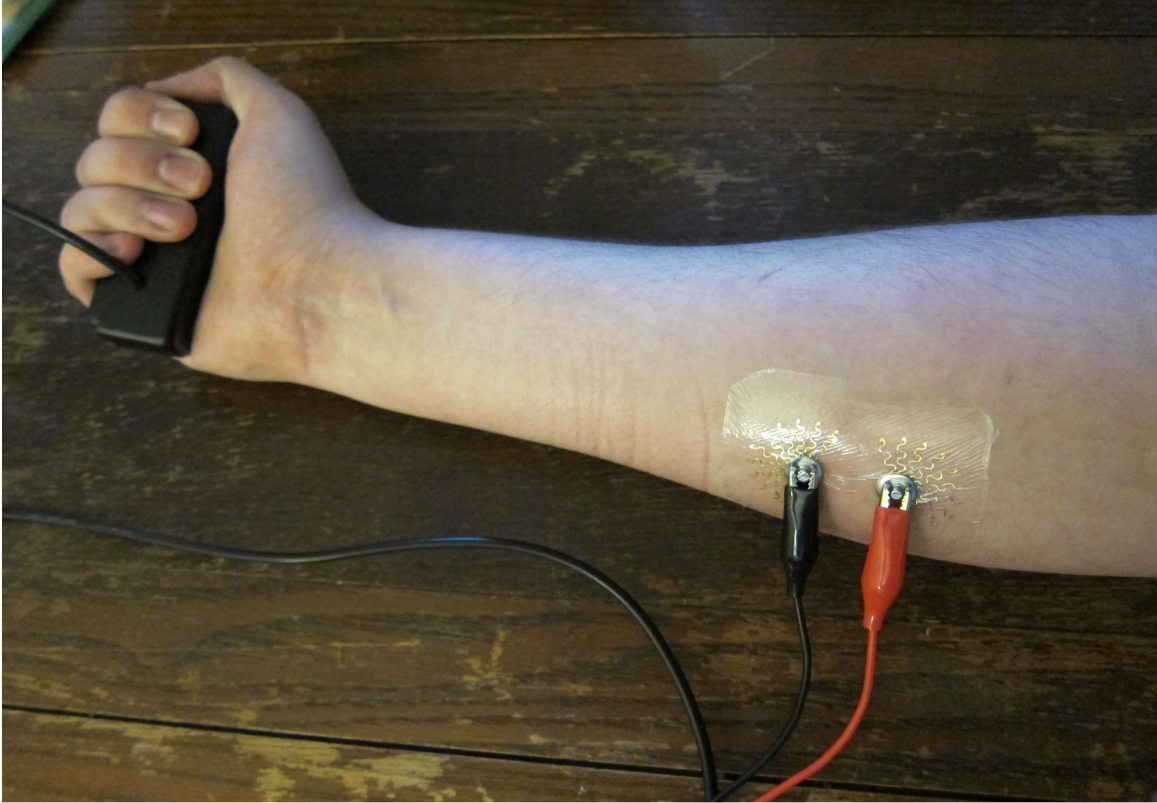


Figure 17: Sun-type Electrode on Arm with Hand Grip Device, and Example Measurement Outputs

During all tests, the subject was asked to perform Maximum Voluntary Contraction (MVC) hand grips, to best induce fatigue and to provide a baseline force to produce. All EMG samples were collected at a sampling rate of 1000 Hz, in order to fully capture the dynamics of the muscle (which are between 50-400 Hz) [37]. All HGF samples are collected at sampling rate of 100 Hz, then up-sampled using sinc interpolation to create an effective sampling rate of 1000 Hz, in order to synchronize with the EMG samples. While no new information is created by up-sampling the data, it allows synchronization without down-sampling EMG, which would cause loss of information in the muscle signals. Subjects tested were all healthy adult males, ages 20-23.

The relationship between forearm EMG and HGF is modeled using ARMAX models. An ARMAX model is a linear model of the form found in Equation 6.

$$X_{1t} = \Phi_{11}X_{1t-1} + \dots + \Phi_{1n}X_{1t-n} + a_{1t} + \theta_{11}a_{1t-1} + \dots + \theta_{1m}a_{1t-m} + \Phi_{22}X_{2t-1} + \dots + \Phi_{2k}X_{2t-k} \quad (6)$$

In Equation 6, the $X_{1(t-i)}$ denotes the output at time $t-i$, $X_{2(t-i)}$ denotes an input at time $t-i$, $a_{1(t-i)}$ denotes normally-distributed white noise associated with input X_1 , and Φ_{ab} and θ_{ab} are constants. Solving for the coefficients of this model allows for prediction of output at time t given the output values at time $(t-1)$ to $(t-m)$ and input values from time $(t-1)$ to $(t-k)$, where m and k are lags set by the operator. Thus this method can be applied to a data sample to return a “predicted” sample set, which is then compared to the real data to track changes in system dynamics. In this Thesis, we use the Kullback-Leibler divergence test to quantify the change in muscle dynamics as the muscle fatigues. In-depth explanation of the algorithm used by this study can be found in the MS by Y. Xie [38].

In all tests, the base ARMAX model was built using the first 10 seconds of the EMG – HGF data, and then its modeling errors were evaluated in a series of successive non-overlapping 10 second windows to gather the Fatigue Index values of each window. Measurements in each test were of one of two different types: Fatiguing Measurements (FM) and Recovery Measurements (RM). Fatiguing Measurements lasted 2 minutes, producing a set of 12 windows. In addition, due to their lengths and the requirement to maintain MVC, FM's also had the effect of fatiguing the muscle involved, meaning no additional exercise of the muscle is necessary to achieve fatigue state. Recovery Measurements last 10 seconds each, producing a single window to evaluate the RM's performance relative to the original fatigue model. The reason for the brevity of these experiments is to avoid additional fatiguing of the muscle; RM's are utilized to track the recovery of a previously-fatigued muscle over time, so avoidance of additional fatigue that may affect results is critical.

Subjects are asked not to exercise or otherwise exert their arm for a full 24 hours prior to testing. During experimental trials, subject is allowed to rest in between data measurements and disconnected from data gathering devices, but both the Sun and conventional electrodes remain on the arm for the duration of the testing period. Fresh electrodes are placed directly over the forearm flexor muscles at the beginning of testing. An additional conventional electrode is placed elsewhere on the body, usually the opposite arm or the leg, to serve as a common ground. Each set of EMG data produces its own ARMAX model, and is only compared to that ARMAX model to determine fatigue. Thus, inherent differences in electrode design or placement would

not affect fatigue values within each measurement, as there is no cross-referencing of models.

Section 4.3: Results and Discussion

In this section, various tests are performed to gauge the effectiveness of the ARMAX modeling strategy for quantifying forearm flexor muscle fatigue, and also to compare the results between Conventional and Sun type electrodes to determine if significant differences in data quality and modeling is present between the two types.

The goal of the first test is to measure the process of fatigue, then track the recovery of the arm back to its initial state. The test subject was asked to perform one Fatiguing Measurement (FM), followed by a Recovery Measurement (RM) every 10 minutes until all arm soreness had dissipated. The results are present in Figure 18.

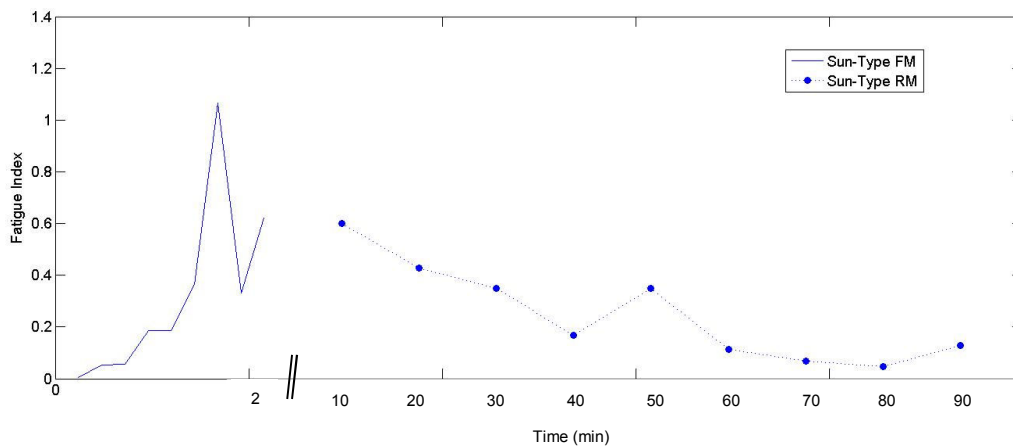


Figure 18: Fatigue and Recovery of Forearm Muscle for Sun-type Electrodes

As can be seen in the figure, the Sun EKG produced an expected FM curve, which begins at no fatigue and quickly rises as the experiment continues and the subject's arm

experiences fatigue, leading to a change in the muscle system dynamics. During recovery, a very clear trend is apparent in which the muscle's Fatigue Index (FI) trends linearly back down to resting state (FI ~ 0), which in this case occurred at 1.5 hours after the initial FM.

While the stretchable-type thin film sensors have already been proven to work equal to or better than conventional electrodes for biopotential collection in Section 3, a redundant test was performed to ensure that electrode type does not have significant effect on fatigue modeling. A test was performed on the same subject the next day, once the arm had fully recovered. The procedure remained the same, except that conventional electrodes were used for EMG collection rather than the Sun-type electrode. The resulting graph of fatigue index is shown in Figure 19.

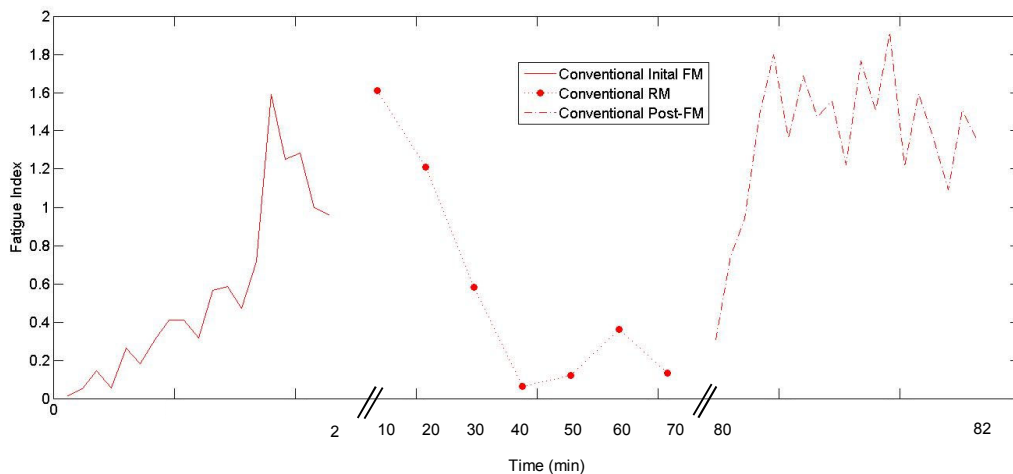


Figure 19: Fatigue and Recovery of Forearm Muscle for Conventional Electrodes

The conventional electrodes clearly demonstrate the same ability to track the measure of fatigue during the trials, as well as track recovery of the muscle back to a resting

state. Based on these data, we can justify that the Sun-Type stretchable sensor performs comparably to conventional electrodes for fatigue monitoring. With this knowledge, the Sun-Type was used for our remaining tests, as it provided better durability and more comfort for the test subject when compared to conventional electrodes. Further analysis between Sun-type and conventional electrodes pertaining to modeling quality is pursued later in this section.

In order to observe the effects of muscle fatigue on a sustained trial, another experiment is performed. The subject begins fully rested, and is then asked to perform an FM trial. At 10 and 20 minutes afterwards, the subject performs one RM trial. Finally at 30 minutes after the initial FM, the subject performs another FM trial. This second FM begins while they are still fatigued from the initial FM trial, based on previous observations with the same subject and subjective confirmation by the subject on arm soreness. The resulting data is contained in Figure 20.

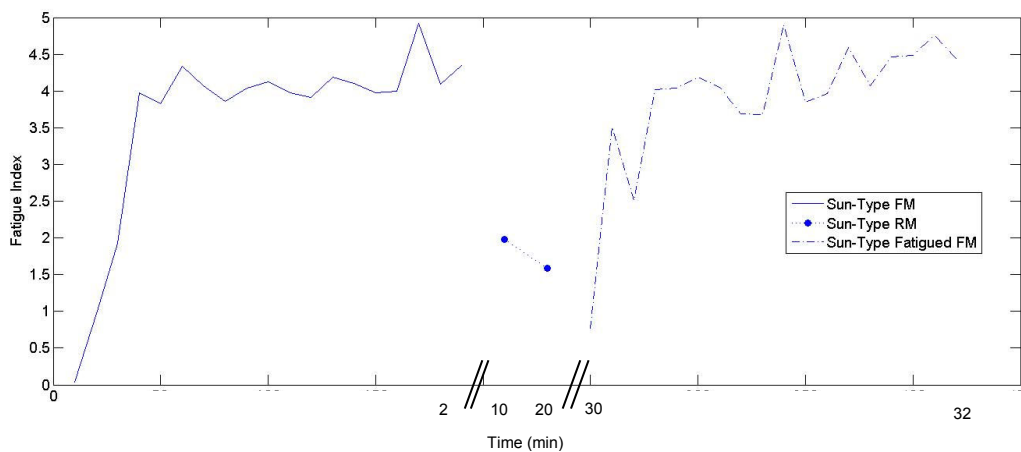


Figure 20: Fatigue and Partial-Recovery of Forearm Flexor Muscle

The results for this experiment follow the expected pattern set by our initial fatigue and recovery trials. The arm begins at a rested state, and fatigues over the course of the

first FM. During recovery, we clearly visualize a steady downward trend, which if continued would lead back to resting state, similar to the results of Figure 17. The second FM measurement begins where the next RM would have been, validating its initial state. However due to the exertion caused by the second RM, the fatigue quickly explodes from that point to beyond the initial FM fatigue. These experimental trials ensure that the FM measurements taken at the “rested” states are indeed distinct from those taken during recovery, and as such can be used to measure and quantify rate of fatigue during muscle exertion.

To test the repeatability of the recovery mechanism, a third series of testing is performed. In this test, the subject begins fully rested. A single FM trial is then performed. Every 10 minutes after the initial FM trial, an RM trial is performed, repeating until the subject expresses no soreness in the testing muscles. At that point, another FM is performed. Following this second FM, RM trials are performed every 10 minutes similar to before, again until no soreness is felt within the muscle. Finally, a last FM trial is performed. The results of this trial can be viewed in Figure 21.

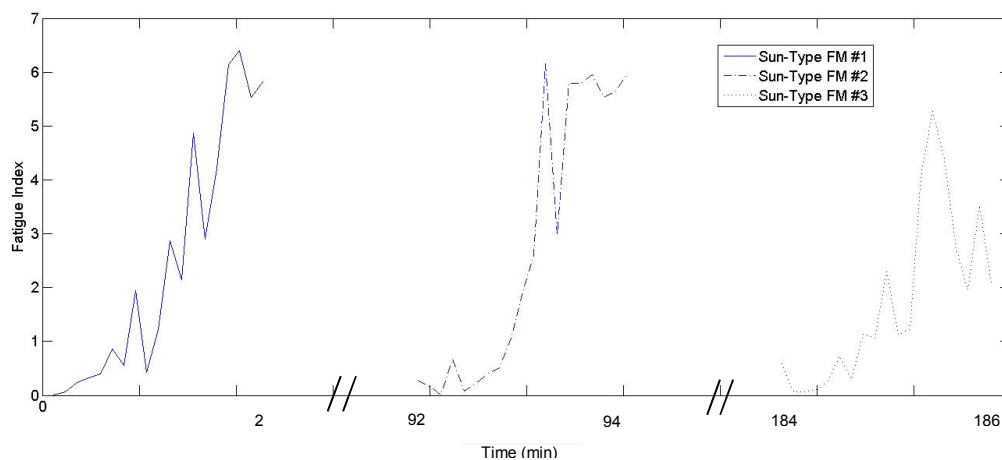


Figure 21: Repeated Fatigue and Recovery of Forearm Flexor Muscles

The repeatability of the muscle is very apparent in the measurements, where each cycle of FM begins at the same rested state, and increases up to a similar limit. as fatigue is induced. This shows that the Fatigue Index method is reliable for long-term measurements involving multiple fatigue states, and is not dependent on previous results.

To investigate further into any potential differences between Sun-Type and conventional electrodes, the ARMAX models used in the fatigue modeling are analyzed.

Representative samples are selected and the ARMAX model used for each of the Sun and Conventional data was extracted and tested versus its constituent data. The validity of the model was determined using a correlation of residuals between the inputs and the outputs, as well as an autocorrelation of the residuals of the output. In an ideal case for ARMAX modeling, the residuals will be independent of one another, and the correlation will be zero in all cases. Alpha was selected as 2%, and the residuals are plotted in Figure 22.

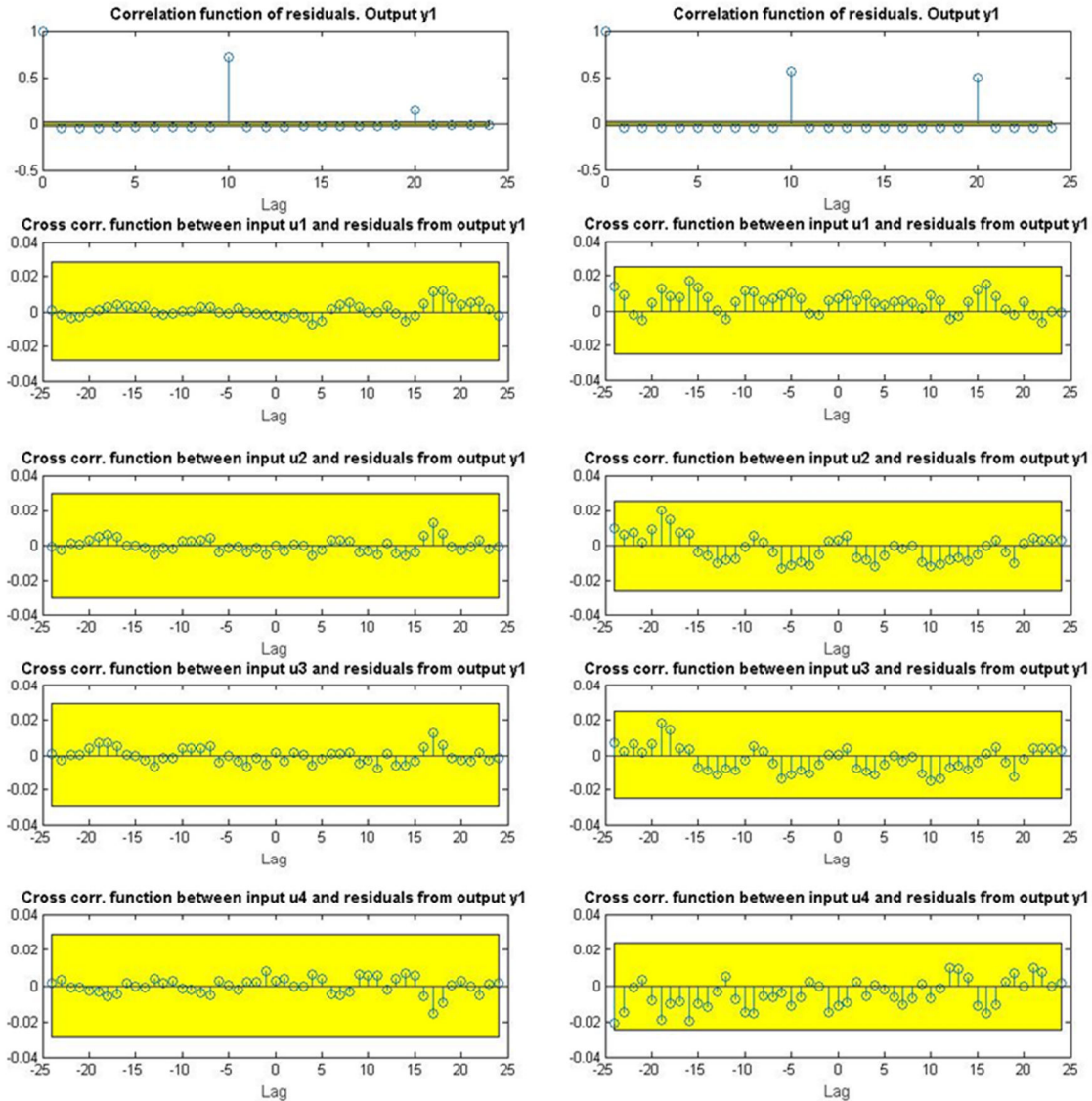


Figure 22: Correlation Residuals for Left) Sun-Type and Right) Conventional Electrode Measurements

In all cases, the residuals remain within the acceptable tolerance range, and thus the ARMAX models for both the Sun type and Conventional data are considered valid. Comparing between the two electrode types, it is clearly visible that the Sun-type electrodes experience much less deviation from the zero comparative to the conventional electrodes. This substantiates the conclusion that for the purposes of ARMAX modeling of forearm flexor muscle fatigue, the Sun type electrode and its

unique stretchability and conformability properties is superior to conventional Ag/AgCl electrodes.

Section 5: Conclusion

In conclusion, the field of stretchable electronics has much room to grow and innovate, and the methodology and results demonstrated in this paper have advanced the capabilities of the field. This paper both introduces a new method of manufacturing stretchable sensors, and a novel use for stretchable sensors in muscle monitoring.

A novel Cut-and-Paste manufacturing method has been developed and investigated for the purpose of producing stretchable electronics. The limits of the manufacturing process have been investigated and tested, including multiple different materials for both the device and the substrate. The versatility of the manufacturing method is demonstrated with the production of a wide variety of sensors, including EP, skin temperature, skin hydration, and strain sensors. Ultimately, the devices produced from the Cut-and-Paste manufacturing method are proven to operate as well or better than conventional devices of the same kind, while also being much quicker and cheaper to produce than traditional microfabrication. Overall the Cut-and-Paste manufacturing method serves to improve research and industry when it comes to producing stretchable sensors.

As a demonstration of the stretchable sensors we produced, the ability to quantify muscle fatigue, particularly the forearm flexor muscles during hand gripping, was investigated. Data of both forearm EMG and corresponding hand grip force were collected and modeled using an ARMAX model system, in order to analyze the relationship between the two parameters. Both a stretchable Sun design electrode and conventional Ag/AgCl electrodes were used in order to compare the performance

between the two types of electrodes. The Kullback-Leibler Divergence test was used to quantify the change in muscle-force dynamics indicating fatigue. Several tests were performed, during which both fatigue and recovery of the muscle was tracked and demonstrated. In all cases, the Sun electrode provided useful and obvious trends to measure fatigue. Analysis of the ARMAX model was also performed by using correlation of residuals, and found the Sun type model to be more valid than the corresponding Conventional model.

In summary, stretchable electronics are a valid and useful tool in physiological research, and the manufacturing and testing methods demonstrated in this paper provide a novel and useful approach to using stretchable electronics in innovative research applications.

References

1. Gilleo, K. (1998). *Handbook of Flexible Circuits (1992 ed.)*. New York, NY: Springer.
2. Harris, K. D., Elias, A. L., & Chung, H. J. (2016). Flexible electronics under strain: A review of mechanical characterization and durability enhancement strategies. *Journal of Materials Science*, 51(6), 2771-2805. <http://dx.doi.org/10.1007/s10853-015-9643-3>
3. Park, S., Vosguerichian, M., & Bao, Z. (2013). A review of fabrication and applications of carbon nanotube film-based flexible electronics. *Nanoscale*, 5(5), 1727-1752. <http://dx.doi.org/10.1039/c3nr33560g>
Published:2013
4. Lipomi, D. J., & Bao, Z. (2011). Stretchable, elastic materials and devices for solar energy conversion. *Energy & Environmental Science*, 4(9), 3314-3328. <http://dx.doi.org/10.1039/c1ee01881g>
5. Sekitani, T., & Someya, T. (2010). Stretchable, large-area organic electronics. *Advanced Materials*, 22(20), 2228-2246. <http://dx.doi.org/10.1002/adma.200904054>
6. Benight, S. J., Wang, C., Tok, J. B. H., & Bao, Z. (2013). Stretchable and self-healing polymers and devices for electronic skin. *Progress in Polymer Science*, 38(12), 1961-1977. <http://dx.doi.org/10.1016/j.progpolymsci.2013.08.001>

7. Xiang, Y., T, L., Suo, Z., & Vlassak, J. (2005). High ductility of a metal film adherent on a polymer substrate. *Applied Physics Letters*, 87(16).
<http://dx.doi.org/10.1063/1.2108110>
8. Li, T., & Suo, Z. (2006). Deformability of thin metal films on elastomer substrates. *International Journal of Solids and Structures*, 43(7-8), 2351-2363.
<http://dx.doi.org/10.1016/j.ijsolstr.2005.04.034>
9. Suo, Z., Ma, E., Gleskova, H., & Wagner, S. (1999). Mechanics of rollable and foldable film-on-foil electronics. *Applied Physics Letters*, 74(8), 1177-1179.
<http://dx.doi.org/10.1063/1.123478>
10. Yao, S., & Zhu, Y. (2015). Nanomaterial-enabled stretchable conductors: strategies, materials and devices. *Advanced Materials*, 27(9), 1480-1511.
<http://dx.doi.org/10.1002/adma.201404446>
11. Sun, Y., & Rogers, J. A. (2007). Structural forms of single crystal semiconductor nanoribbons for high-performance stretchable electronics. *Journal of Materials Chemistry*, 17(9), 832-840.
12. Lu, N., & Yang, S. (2015). Mechanics for stretchable sensors. *Current Opinion in Solid State & Materials Science*, 19(3), 149-159.
<http://dx.doi.org/10.1016/j.cossms.2014.12.007>
13. Cheng, T., Zhang, Y., Lai, W.-Y., & Huang, W. (2015). Stretchable thin film electrodes for flexible electronics with high deformability and stretchability. *Advanced Materials*, 27(22), 3349-3376.
<http://dx.doi.org/10.1002/adma.201405864>

14. Arumugam, V., Naresh, M., & Sanjeevi, R. (1994). Effect of strain-rate on the fracture-behavior of skin. *Journal of Biosciences*, 19(3), 307-313.
<http://dx.doi.org/10.1007/BF02716820>
15. McGrath, J. A., Eady, R. A., & Pope, F. M. (2004). *Rook's textbook of dermatology* (7th ed.). Blackwell.
16. Yamamoto, T., & Yamamoto, Y. (1976). Electrical properties of the epidermal stratum corneum. *Medical and Biological Engineering*, 14(2), 151-158.
<http://dx.doi.org/10.1007/BF02478741>
17. Cram, J., & Rommen, D. (1989). Effects of skin preparation on data collected using an EMG muscle-scanning procedure. *Biofeedback and Self-Regulation*, 14(1), 75-82. <http://dx.doi.org/10.1007/BF00999342>
18. Smith, C. M., Housh, T. J., Herda, T. J., Zuniga, J. M., Ryan, E. D., Camic, C. L., ...Johnson, G. O. (2015). Effects of the innervation zone on the time and frequency domain parameters of the surface electromyographic signal. *Journal of Electromyography and Kinesiology*, 25(4), 565-570.
19. Yeo, W.-H., Kim, Y.-S., Lee, J., Ameen, A., Shi, L., Li, M., . . . Rogers, J. A. (2013). Multifunctional epidermal electronics printed directly onto the skin. *Advanced Materials*, 25(20), 2773-2778.
<http://dx.doi.org/10.1002/adma.201204426>
20. Coupin, H. (1901). On the toxicity of compounds of silver, mercury, gold, platinum and palladium. *Comptes Rendus Des Seances De La Societe De Biologie Et De Ses Filiales*, 53, 509-510.

21. Edwards, R. H. T. (1981). *Human muscle function and fatigue*. Chichester, UK: John Wiley & Sons. <http://dx.doi.org/10.1002/9780470715420.ch1>
22. Enoka, R. M., & Duchateau, J. (2008). Muscle fatigue: What, why and how it influences muscle function. *Journal of Physiology - London*, 586(1), 11-23. <http://dx.doi.org/10.1113/jphysiol.2007.139477>
23. De Luca, C. (1984). Myoelectrical manifestations of localized muscular fatigue in humans. *CRC Critical Reviews in Biomedical Engineering*, 11(4), 251-279.
24. Cifrek, M., Medved, V., Tonkovic, S., & Ostojic, S. (2009). Surface EMG based muscle fatigue evaluation in biomechanics. *Clinical Biomechanics*, 24(4), 327-340. <http://dx.doi.org/10.1016/j.clinbiomech.2009.01.010>
25. Hagg, G. (1981). Electro-myographic fatigue analysis based on the number of zero crossings. *Pflugers Archiv-European Journal of Physiology*, 391(1), 78-80. <http://dx.doi.org/10.1007/BF00580699>
26. Roy, S., De Luca, C., Snydermackler, L., Emley, M., Crenshaw, R., & Lyons, J. (1990). Fatigue, recovery, and low back pain in varsity rowers. *Medicine and Science in Sports and Exercise*, 22(4), 463-469.
27. Paiss, O., & Inbar, G. (1987). Autoregressive modeling of surface EMG and its spectrum with application to fatigue. *IEEE Transactions on Biomedical Engineering*, 34(10), 761-770. <http://dx.doi.org/10.1109/TBME.1987.325918>
28. Merletti, R., & Loconte, L. (1995). Advances in processing of surface myoelectric signals. *Medical & Biological Engineering & Computing*, 33(3), 362-372.

29. Cifrek, M., 1997. Myoelectric Signal Analysis during Dynamic Fatigue. Ph.D. Dissertation. University of Zagreb, Faculty of Electrical Engineering and Computing (in Croatian).
30. Korosec, D. (1999). Continuous time-varying autoregressive spectrum for assessment of fatigue induced changes in SEMG signals. *Engineering in Medicine and Biology*, 1.
31. Knaflitz, M., & Bonato, P. (1999). Time–frequency methods applied to muscle fatigue assessment during dynamic contractions. *Journal of Electromyography and Kinesiology*, 9(5), 337-350. [http://dx.doi.org/10.1016/S1050-6411\(99\)00009-7](http://dx.doi.org/10.1016/S1050-6411(99)00009-7)
32. Lu, N., Wang, X., Suo, Z., & Vlassak, J. (2007). Metal films on polymer substrates stretched beyond 50%. *Applied Physics Letters*, 91(22). <http://dx.doi.org/10.1063/1.2817234>
33. Seitz, H., Marlovits, S., Schwendenwein, I., Muller, E., & Vecsei, V. (1998). Biocompatibility of polyethylene terephthalate (Trevira (R) hochfest) augmentation device in repair of the anterior cruciate ligament. *Biomaterials*, 19(1-3), 189-196. [http://dx.doi.org/10.1016/S0142-9612\(97\)00201-9](http://dx.doi.org/10.1016/S0142-9612(97)00201-9)
34. Jeong, J.-W., Yeo, W.-H., Akhtar, A., Norton, J. J. S., Kwack, Y.-J., Li, S., ...Rogers, J. A. (2013). Materials and optimized designs for human-machine interfaces via epidermal electronics. *Advanced Materials*, 25(47), 6839-6846. <http://dx.doi.org/10.1002/adma.201301921>

35. Widlund, T., Yang, S., Hsu, Y.-Y., & Lu, N. (2014). Stretchability and compliance of freestanding serpentine-shaped ribbons. *International Journal of Solids and Structures*, 51(23-24), 4026-4037.
36. Miranda de Sa, A. M. F. L., de Seixas, J. M., Costa, J. D., Jr, Ferreira, D. D., & Cerqueira, A. S. (2015). A principal component-based algorithm for denoising in single channel data (PCA for denoising in single channel data). *Measurement*, 60, 121-128.
<http://dx.doi.org/10.1016/j.measurement.2014.09.079>
37. Viitasalo, J., & Komi, P. (1977). Signal characteristics of EMG during fatigue. *European Journal of Applied Physiology and Occupational Physiology*, 37(2), 111-121. <http://dx.doi.org/10.1007/BF00421697>
38. Xie, Y. (2016). *A model based approach for evaluating human neuromusculoskeletal system performance* (Unpublished master's thesis). University of Texas at Austin, Austin, TX.